TOWARD HIGH PERFORMANCE NANOCARBON FIBERS

A Thesis
presented to
the Faculty of California Polytechnic State University,
San Luis Obispo

In Partial Fulfillment
of the Requirements for the Degree
Master of Science in Polymers and Coatings Science

by
Michaela R. Pfau
March 2016

COMMITTEE MEMBERSHIP

TITLE: Toward High Performance Nanocarbon Fibers

AUTHOR: Michaela R. Pfau

DATE SUBMITTED: March 2016

COMMITTEE CHAIR: Shanju Zhang, Ph.D.
Assistant Professor of Chemistry

COMMITTEE MEMBER: Ray Fernando, Ph.D.
Endowed Chair of Polymers and Coatings

COMMITTEE MEMBER: Philip Costanzo, Ph.D.
Associate Professor of Chemistry

ABSTRACT

Toward High Performance Nanocarbon Fibers

Michaela R. Pfau

High performance carbon fibers (CFs) have been a commercially available since their commercial boom in the 1970s, and are generally produced via carbonization of poly (acrylonitrile) (PAN). More recently, carbon nanomaterials like graphene and carbon nanotubes (CNTs) have been discovered and have shown excellent mechanical, thermal, and electrical properties due to their sp^2 carbon repeating structure. Graphene and CNTs can both be organized into macroscopic fibers using a number of different techniques, resulting in fibers with promising mechanical performance that can be readily multifunctionalized. In some cases, the two materials have been combined, and the resulting hybrid fibers have been shown to display synergistically enhanced mechanical properties. The incredible intrinsic properties of graphene and CNTs has never been fully realized in their fiber assemblies, so part of the aim of this work is to discover methods to improve upon the performance of nanocarbon based fibers. Carbon nanomaterials can be difficult to work with because of the difficulty in processing them into commercially viable materials, and the challenges associated with scalable production techniques. So, the main goal of this work is to prepare hybrid graphene and CNT based fibers with optimal mechanical performance using simple, cost-effective methods.

ACKNOWLEDGMENTS

First off, I would like to thank my primary advisor, Dr. Shanju Zhang for mentoring me and for always pushing me to excel. I would also like to thank my committee members Dr. Ray Fernando for introducing me to the Polymers & Coatings program, and Dr. Phillip Costanzo for his continued advisement regarding both research and future opportunities.

I want to thank everyone in my group. Particularly, I would like to thank past members Grace Luo, Greg Braggin, and Alix Stevenson for their contributions to this project, and to my training. I would also like to thank current group members Karina Reynolds for preparing all of the precursor materials, and Mackenzie Kirkpatrick for continuing work on this project.

In the chemistry department, I want to thank all of the professors and students who assisted me with instrumentation. Thank you to Dr. Gregory Scott and his student Matt de Silva for their support, and to Dr. Eric Jones. I would also like to thank professors from the materials engineering department- without them, none of the imaging would have been possible. So, thank you to Dr. Trevor Harding, and to Dr. Richard Savage.

I would like to thank our collaborators Dr. Juan Josè Villatela at the IMDEA Materials Institute in Madrid for providing precursor materials.

None of this work would have been possible without the Polymers & Coatings program and the Kenneth N. Edward Western Coatings Technology Center, or without funding from National Science Foundation, the Bill Moore Student Fellowship, and the Cal Poly Extramural Funding Initiative.

TABLE OF CONTENTS

Page

CHAPTER

LIST OF TABLES

Table Page

LIST OF FIGURES

1. Introduction

There has been a great deal of hype regarding carbon nanomaterials like carbon nanotubes (CNTs) and graphene in recent decades. Both have been shown to have excellent potential in creating materials with highly desirable properties, such as mechanical durability. Unfortunately, there are many challenges associated with producing and processing carbon nanomaterials, and so, publications in the field have far exceeded the number of issued patents as shown in Figure 1.[1] Figure 1 also includes some selected applications of new-age CNT materials. CNTs have been shown to be in the growth phase of their production cycle, so development of commercial applications is expected to continue.[1] Recent advancements have led to lower costs and increased production of CNTs in particular, but production is still about 10 times more expensive for CNT based fibers than for existing carbon fibers (CFs).[1] Suffice to say, developing facile techniques for producing carbon nanomaterial based macroscopic materials is highly desirable.

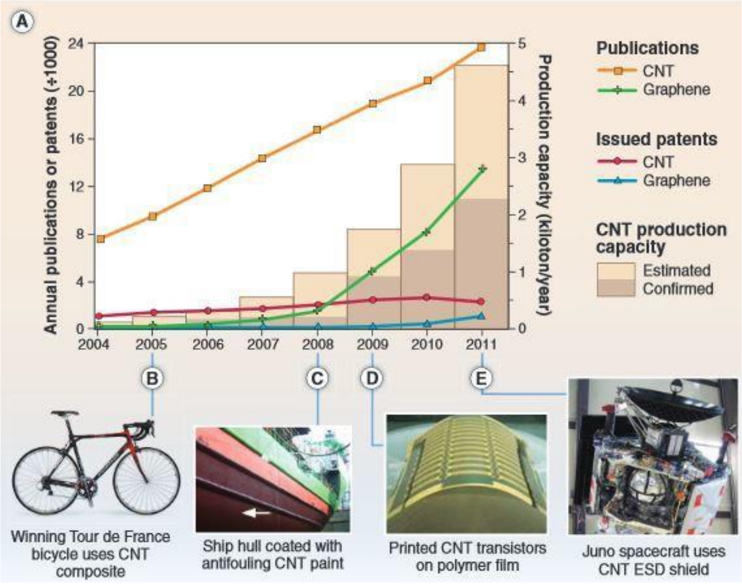

Figure 1. Trends in publications and patents for graphene and CNT, and trends in estimated and confirmed CNT production capacity from 2004 to 2011.[1]

1.1 Carbon Nanomaterials

1.1.1 Graphene, Graphene Oxide (GO), and Reduced Graphene Oxide (rGO)

The structure of graphene consists of a single, monatomic layer of repeating sp^2 carbons organized in a hexagonal lattice.[2] The material gained popularity in 2004 when Novosolev *et al* produced few layered, and single layered graphene via repeated peeling of highly oriented pyrolytic graphite using tape, and prepared thin films that were transferred to silicon substrates for electrical characterization.[2,3] Their technique was dubbed the “Scotch tape method,” and while it remains useful in research for producing pristine sheets of graphene, it does not have the potential to scale-up.[2,4] Graphene’s unique structure yields unique physiochemical properties such as mechanical strength, thermal stability, and electrical conductivity making graphene of interest for a wide array of applications including polymer composites, energy-related materials, and biomedical materials.[2] Specifically, graphene has been shown to have a tensile strength of up to 130 GPa, with an elastic modulus of 1.1 TPa.[5] Additionally, graphene’s small size and monatomic thickness makes it of interest as a nanomaterial building block.[6] So, other methods for producing graphene such as mild exfoliation, growth on silicon carbide, and chemical vapor deposition (CVD) using transition metal substrates have all been investigated, but they all present difficulties.[7] A more low-cost and scalable method is to prepare graphene oxide (GO) from graphite followed by thermal or chemical reduction.[7]

Interestingly enough, GO was first studied more than 150 years ago in 1859 by Brodie who mixed flake graphite with fuming nitric acid (HNO_3) and potassium chlorate ($KClO_3$).[2,8] Brodie’s goal was to find the molecular weight of his product, which was not possible due to GO’s indeterminate structure, but he did observe a mass increase after oxidation, followed by a mass decrease when the product was heated to 220°C.[2] When graphite is combined with oxidizing agents, defects in the sp^2 lattice structure serve as nucleation sites for functionalization, and the resulting product includes oxygen containing functional groups.[2] The introduction of oxygen groups causes changes in the structure of GO when compared to graphene.

In some cases, the structural differences of GO can be advantageous. For instance, one major challenge in working with graphene is that, because of the strong Van der Waals interactions (5.9 kJ/mol C) between sheets, the sheets can be difficult to separate, and they are not dispersible in many solvents, which makes graphene a difficult material to process.[3] The addition of oxygen functionality makes GO easily dispersible in a number of common solvents including water. Other structural differences of GO can detract from the unique properties observed in graphene, like the incorporation of sp^3 carbons into the lattice, which disrupts the pi-network leading to a lower conductivity than graphene.[2] Mechanical strength may also be compromised because sheets of GO do not interact as favorably with one another and cannot stack as tightly as sheets of graphene do.

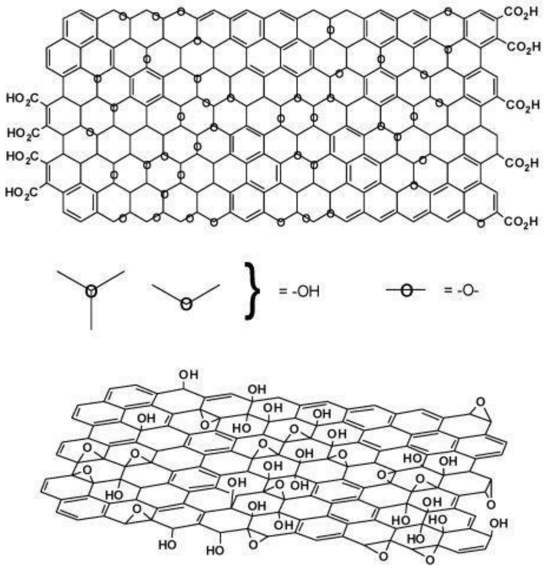

Figure 2. The Lerf-Klinowski models of GO.[2]

The precise structure of GO has not been determined, but various models have been proposed that address how the hexagonal lattice is affected by functionalization, as well as what type of functional groups are added, and how they are distributed.[2] Individual samples can vary considerably, plus GO's structure is ambiguous and berthollide, meaning GO has a nonstoichiometric composition, making GO a difficult material to characterize.[2] Early models relied heavily on elemental composition and reactivity tests, and often proposed some sort of repeat unit structure, but Lerf *et al* proposed an ambiguous structure in 1998 based on solid-state nuclear magnetic resonance spectroscopy (NMR) as shown in Figure 2.[9] The Lerf-Klinowski model includes two possible structures due to the ambiguity of whether or not carboxylic acid groups exist along the edges of the GO sheets.[9] Lerf and coworkers performed further work using reactivity analyses and discovered that the double bonds are likely conjugated or aromatic, rather than isolated, that the dominant functional groups on the surface are tertiary alcohols and 1,2-ethers, and that carboxylic acids were only present in low quantities along the edges in addition to ketone groups.[2] This work improved upon previous models, in that, it did not propose a regular distribution of functional groups.[2] Additionally, previous work had suggested that 1,3-ethers existed on the basal plane but Lerf and coworkers realized that the formation 1,3-ethers required a complex sequence of reactions that would not be likely to occur under the reaction conditions.[9] In 2010, Lee *et al* used a variety of analytical techniques and proposed a different structure that refuted some aspects of the Lerf-Klinowski model.[10] Lee and coworkers did not find any evidence of carboxylic acid groups suggesting only ketone groups are found on the periphery of GO sheets, and they determined that the hydroxyl groups lie on opposite sides of the basal plane due to repulsion.[10] In short, no unambiguous model for GO exists, and results may be affected by graphite source and type of oxidation methods used, but the overall structure of GO likely consists of some carboxylic acid and ketone groups on the edges, with hydroxyl, epoxide (1,2-ether) groups, and conjugated or aromatic double bonds in the basal plane.[2]

GOs behavior in solvents depends primarily on the type of solvent, and the extent of functionalization. With more functionality comes greater polarity of GO, which allows the sheets to interact favorably in polar solvents like water. Studies performed on the dispersability of GO have shown that the most stable dispersions occur in water, dimethylformamide (DMF), and *N*-methyl-2-pyrorolidone (NMP).[11] Ethanol (EtOH), propanol, dimethyl sulfoxide (DMSO), and pyridine all had short term stability where precipitation was observed in a matter of hours or days, and tetrahydrofuran (THF) and ethylene glycol were slightly more stable with only a small amount of observed precipitation.[11] GO has a high surface area of hydrogen bonding to itself, so molecules like EtOH are unable to solvate GO sheets.[11] In most cases, GO is thought of as being hydrophilic, but because most of the oxygen functionality exists along the edges of GO sheets, GO can be thought of as an amphiphile with hydrophilic edges and a mostly hydrophobic basal plane.[12] GO has the ability to adsorb on interfaces and to lower surface tension, just as surfactants do.[12] The amphiphillicity of GO can be altered by the size of the GO sheets, and by pH, because as pH is increased, the carboxylic acid groups are deprotonated and the polarity of the GO sheets is increased.[12] GO has even been shown to effectively disperse other nonpolar carbonaceous materials like graphite and carbon nanotubes (CNTs).[12]

As previously mentioned, the method used to prepare GO can have an impact on its structure. Brodie's original method using fuming HNO_3 and $KClO_3$ was effective, because the oxidizing agents are strong, but $KClO_3$ is known to be explosive, so other less hazardous preparations were investigated by Hummers and Offeman in 1958.[8]

They used a mixture of concentrated sulfuric acid (H_2SO_4) and potassium permanganate ($KMnO_4$), and were able to achieve a similar degree of oxidation.[12] In this work, a modified Hummers' method will be used to prepare GO from flake graphite. It is worth noting that the actual active species is dimanganese oxide (Mn_2O_7), which is formed when $KMnO_4$ is combined with H_2SO_4.[2] There are still some dangers in using this method as Mn_2O_7 is known to detonate at temperatures greater than 55°C.[2] Studies have shown that Mn_2O_7 selectively oxidizes aliphatic double bonds over aromatic double bonds.[2] The exact mechanism of oxidation is unknown, but this provides some insight by suggesting that oxidation mostly occurs at existing defects in the flake graphite, rather than at intact sp^2 carbon networks.[2] Current ways to prepare GO often combine tactics from existing methods, and often include intermediate steps where graphene intercalated compounds (GICs) and expanded graphite (EG) are formed. GICs are formed when molecules, such as sulfate, intercalate between the layers of graphene and allow high heat treatment to exfoliate the graphite in such a way that the volume expands significantly to produce EG.[2,13] EG has a much higher surface area than graphite and can be more effectively oxidized into single layer GO.[2,13]

GO can then be reduced, chemically or thermally, in order to produce reduced graphene oxide (rGO).[2] Choosing chemicals to reduce aqueous dispersions of GO can be challenging because many strong reducing agents react with water.[2] Hydrazine monohydrate is a common choice for reducing GO because it does not react with water, and it effectively reduces oxygen functional groups, but it also causes hetero-atomic contamination because nitrogen containing groups are added to the sheets during this process.[2] Also, hydrazine is highly flammable and corrosive making it a dangerous chemical to handle.[14] An alternative choice investigated more recently is NMP. NMP has a high boiling point so there are less risks associated with the process, and NMP has oxygen-scavenging properties making it an ideal candidate for producing rGO.[14] An added benefit to using NMP is that it can act as a dispersant making processing of rGO more simple, and it can be removed from final products via annealing.[14] GO can also be thermally treated to produce rGO. Many reports use temperatures over 1000°C to produce rGO via thermal reduction.[2] At high temperatures, the oxygen functionalities are removed as CO_2, and high temperatures lead to high pressure that forces individual sheets apart, so most rGO produced this way is single-layered.[2] Using excessively high temperatures is effective in reducing GO, but a lot of damage to the sheets can occur. Most oxygen functionalities cannot be reduced at temperatures lower than 200°C, so in this study a thermal reduction at 250°C will be used.[14]

Producing rGO from GO causes the formation of defects leading to less optimal properties in rGO compared to graphene. For instance, the hydrazine reduction method leaves a lot of bound nitrogen functionalities, and the resulting sp^3 carbons disrupt the pi-network leading to lower conductivity.[2] Thermal methods are known to cause vacancies and topological defects that can also cause a decrease in conductivity, and while it has not been quantified, these defects are also thought to have a negative impact on mechanical properties.[2] Transmission electron microscopy (TEM) has been used to better understand the structure of rGO, and it has been determined that about 60% of the surface consists of crystallized hexagonal lattice graphene, about 30% is contaminated with adsorbents and the structure beneath cannot be determined, and about 5% consists of defects.[7] Pentagon-heptagon pairs and quasi-amorphous single layered C were the most common types of topological defects, and they also appeared to distort the intact regions nearby.[7] Even though the defects covered a small area, they did appear to cause a significant amount of strain on the lattice.[7] Remaining oxygen functionality can also cause less than optimal properties, but even if the GO is effectively reduced, properties may still be compromised due to stress-causing defects.[7] The lack of oxygen functionality in rGO causes it to behave more like graphene in solvents. Due to the strong VDW between sheets of rGO, it is not known to form stable dispersions in anything aside from DMF.[15] Overall, preparing GO is useful for simple processing, and even though the final rGO product does have the disadvantage of containing defects, this is still the most cost-effective and scalable technique for preparing graphene-like materials.

1.1.2 Carbon Nanotubes (CNTs) and oxidized CNTs (oCNTs)

Carbon nanotubes (CNTs) were first produced by Iijima *et al* in 1991, and, like graphene, have since gained popular interest due to their potential as a building block for carbon based nanomaterials.[16] CNTs can be thought of as rolled up sheets of graphene, or seamless cylinders of hexagonally arranged sp^2 carbons that are long and thin.[1] Single-walled CNTs (SWNTs) contain about 10 atoms in their circumference and their diameter is usually about 1-2 nm.[16] Multi-walled CNTs (MWNTs) are made up of concentric cylinders of graphene and have a wider range of diameters ranging from 3 to 30 nm depending on how many walls the CNTs have.[16] The properties of CNTs can also change significantly depending on the axis used to roll the sheet of graphene.[16] The different types of CNTs produced by changing the rolling axis is shown in Figure 3. The orientation of the hexagonal lattice with respect to the tube axis is known to affect the conducting properties of CNTs.[16] Armchair CNTs are metallic while zigzag and chiral CNTs are semi-conducting.[16] There is not currently information regarding how these orientations affect mechanical properties. Another variation for CNTs is whether or not their ends are opened or closed.[16] Closed-end CNTs are known to contain a high number of defects like heptagons and pentagons in the end caps.[16] Like graphene, the unique structure of CNTs leads to optimal conductive, thermal and mechanical properties useful in a wide array of applications.[1] Specifically, SWNTs have been shownto have a Young's modulus as high as 1 TPa, a tensile strength of 63 GPa, and a density as low as 1.3 g/mL.[16] CNTs are roughly 50 times stronger than steel, and about 1/6 as dense making CNTs an excellent potential building block for the fabrication of lightweight, durable materials, such as high performance fibers.[16] However, these incredible intrinsic properties of CNTs have never been fully realized in CNT based materials. Interestingly, while CNTs unique structure lends itself to beneficial properties, it can also be a health concern.[17] The length of CNTs is variable, but MWNTs longer than 20 µm have been shown to mimic the structure, and health hazards, of long fiber amosites (LFAs) commonly known as asbestos.[17] Care should be taken when working with CNTs of this length in powder forms that may be easy to inhale.

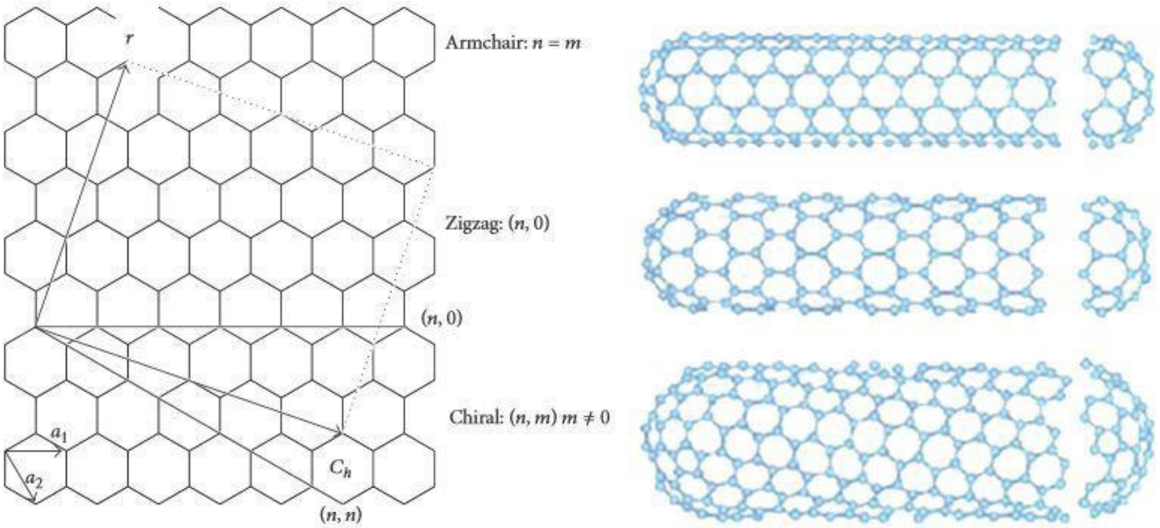

Figure 3. Orientation of CNTs based on graphene rolling axis.[16]

CVD is the dominant synthetic technique used to achieve high-volume production of CNTs.[1,16] The basic procedure involves the decomposition of a volatile carbon containing compound at a temperature below 1200°C, and the use of metallic nanoparticles for catalysis of CNT growth.[16] This method has advantages over other methods, such as arc discharge and laser vaporization, because it is lower in cost, has a higher yield, and the operation does not require as much energy input.[16] Both SWNTs and MWNTs can be produced using CVD, and some control over structural aspects is possible.[16] Additionally, improvements in the CVD method have significantly reduced the cost of producing MWNTs helping to make CNTs more commercially viable.[1] CVD using EtOH as the carbon source has been found to produce an alcohol radical that removes amorphous carbon, which is an added benefit.[16] One major disadvantage to using the CVD method is that the final product contains a large number of defects.[16] But, CNT yarn materials have been directly extruded from the CNT aerogel during CVD demonstrating the scalability of this approach.[16] In this work, a CNT yarn produced directly from an aerogel will be used to prepare fibers.

CNTs are difficult to disperse in common solvents due to the strong VDW interactions between individual rods.[11] One way to overcome the tendency of CNTs to aggregate is to use a superacid as the solvent, but this can be problematic for common processing techniques.[18] Another common approach is to functionalize the CNTs via oxidation.[18] Analogous to GO, oxidized CNTs (oCNTs) have the added benefit of being dispersible, but some of their properties may be negatively affected with the addition of functional groups. A common treatment for preparing oCNTs is to use H_2SO_4 and HNO_3 in a 3:1 ratio, which is the method that will be used in this work.[18] Defects like heptagons and pentagons cause heavy strain, making oxidation more likely to occur at these sites, so the ends of oCNTs are typically more functionalized than the sidewalls.[19] Compared to other oxidants, the combination of H_2SO_4 and HNO_3 was shown to result in a greater degree of oxidation.[19] In one proposed mechanism, NO_2 is formed$^+$ and acts via electrophilic attack to generate active sites like carbonyl or hydroxyl groups at defect sites.[19] Then, the active sites, produced in the previous step, are oxidized resulting in functional groups such as carboxylic acids, and destruction of the graphene structure.[19] When CNTs are oxidized, the ends always become uncapped and the length is typically shortened.[19] Like GO, the exact structure of oCNTs is variable and can depend upon the original source of CNTs, on the type of oxidant used, and on the reaction conditions.[18] Previous studies have shown that H_2SO_4 and HNO_3 reactants result in a large amount of carboxylic acid groups at the edges in addition to some oxygen functionality on the sidewalls.[19,20] Oxidative treatments have also been shown to remove amorphous carbon and metallic impurities.[20] This is advantageous especially because most commercial CNTs have purities as low as 50%.[20] Once treated, oCNTs have been shown to form stable dispersions in all of the previously mentioned solvents that GO forms a stable dispersion in.[11]

1.2 Liquid Crystal (LC) Behavior

Liquid crystals (LCs), also known as a mesophase or mesogen, can be thought of as a fourth state of matter that has shared properties with both solids and liquids.[18] LCs are solid-like in the sense that they have long range order, and they are liquid-like in the sense that they have the ability to flow.[18] This makes LCs unique because their order is susceptible to manipulation and can be controlled by applying an external force such as a magnetic field or a shear force.[18] Certain types of particles will form lyotropic LCs (LLCs), which are concentration dependent.[21] According to Onsager’s theory, anisometric particles will orient themselves into an anisotropic phase above some critical concentration, driven by the entropy of their excluded free volume, and an increase in packing entropy.[22] The more anisometric the particles are, the lower the critical concentration will be.[23] So, above a critical concentration, anisometric particles will selfassemble, which can be advantageous, because many physical properties like electrical, magnetic, and mechanical properties depend on orientation.[18]

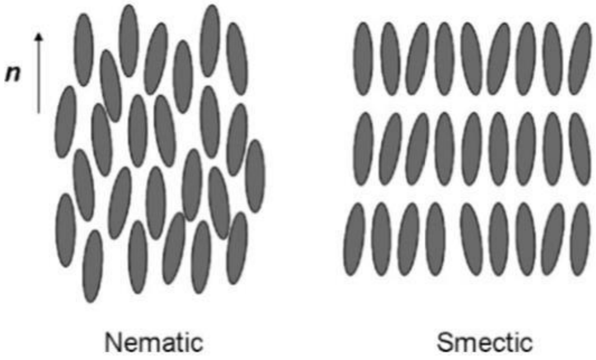

Figure 4. The nematic and smectic phases of LCs.[18]

LCs have 3 phases: isotropic, biphasic and anisotropic.[18] At low concentrations, the particles are randomly distributed in all directions and the dispersion is said to be isotropic.[18] As the concentration is increased a biphase transition may occur where both the isotropic and anisotropic, or LC, phase coexist.[18] In the biphase, microdomains of anisotropy exist, but they are surrounded by the isotropic phase.[18] Once the critical concentration is achieved, the ordered LC phase exists.[18] Due to their anisotropy, LC phases have a unique optical property called birefringence meaning that their refractive index in dependent on the polarization of light.[18] This allows for simple determination of the LC phase transitions using polarized optical microscopy (POM).[18] Using POM, the isotropic phase will appear black, while the LC phase will appear to have a distinct texture whose light and dark regions alter as the polarizer is rotated.[18] Nematic LC phases are characterized by their distinct Schlierien, or brush-like, texture that can be observed using POM.[18] Nematic LCs differ from smectic LCs, in that, the nematic phase consists of particles with orientational order, while the smectic phase consists of particles with both orientational and positional order.[18] A diagram showing the difference between the nematic and smectic phase is shown in Figure 4. For the carbon nanomaterials discussed previously, the nematic phase is much more commonly reported.[18,24]

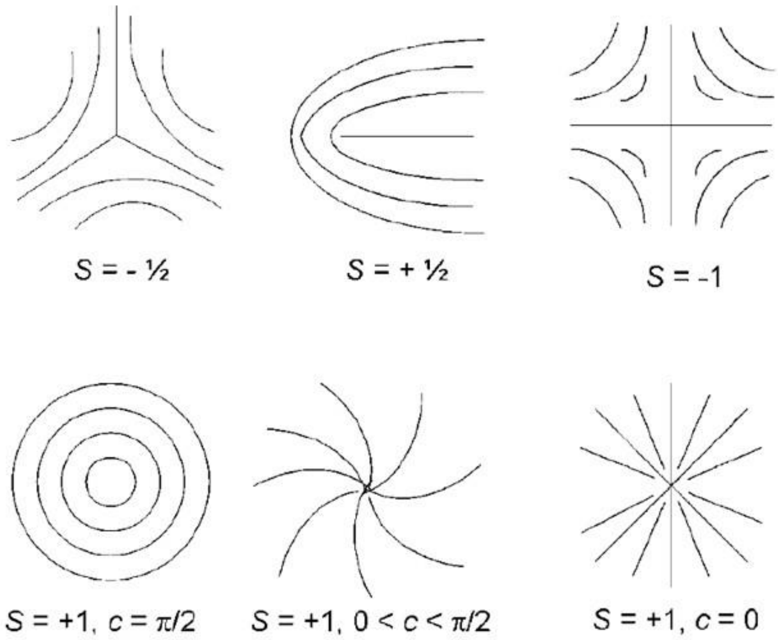

Figure 5. Common disclination microstructures.[18]

It is worth noting that while LLCs are advantageous due to their self-assembling properties, they also include topological defects called disclinations.[25] As shown in Figure 4, LCs orient themselves along a director field, *n*, that depends upon the minimization of total free energy.[25] In disclinations, the director is rotated causing a symmetry- breaking defect.[25] The strength of a disclination depends on the number of rotations of the director, and common examples for LCs are shown in Figure 5.[25] Disclinations with opposite (+/-) signs will attract and eventually annihilate one another, while disclinations with the same sign will repel on another.[25] POM can be used as a simple method to view disclinations in a sample.[18] Disclination cores have high elastic-distortion energy, so for polydisperse samples, smaller particles and contaminants are thought to preferentially occupy the disclinations.[23] Defects like topological disclinations are significant because they can affect the alignment quality of LCs.[18]

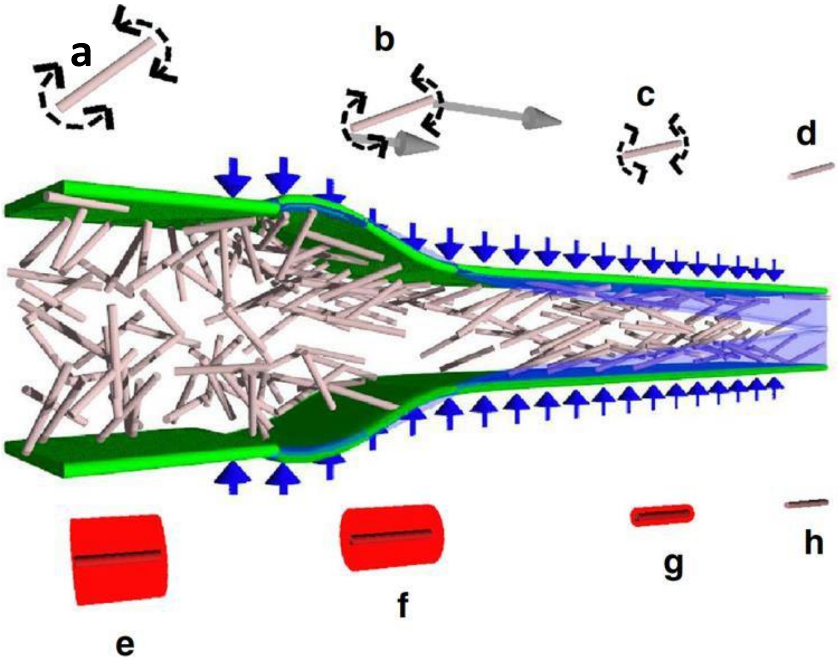

Figure 6. LC alignment in a microfluidic channel.[26]

The use of LCs can have great benefits in commercial applications because they allow for simple processing of materials that can otherwise be challenging to work with.[21] One of the most common examples is with Kevlar fibers. Kevlar is a very rigid polymer and while its rigidity lends itself to beneficial properties like high mechanical and thermal stability, it also makes Kevlar difficult to process into a usable material using common techniques like melt-spinning.[21] But, the use of LCs allows aligned Kevlar fibers to be produced using a simple wet-spinning technique.[21] Similar techniques have been employed with other liquid crystalline materials such as cellulose filaments.[26] Hakansson *et al* used cellulose filament LCs to produce fibers, and increased their alignment with the help of microfluidic channels.[26] As previously mentioned, LCs are susceptible to external forces, and the laminar flow in a microfluidic channel affects how the LC orients itself.[26] A diagram is shown in Figure 6 showing that the particles will align in the direction of the laminar flow.[26] Accelerating the flow was shown to cause greater alignment with respect to the flow, which is significant because fiber strength depends upon alignment with respect to the fiber axis.[27] While microfluidic channels can help to align the nematic LCs, surface stabilized disclinations may form due to interactions with the channel surface.[28] These can cause flow-induced defects that vary with flow velocity and channel width, and can impact the morphology of fibers produced in this way.[28]

1.2.1 LCs of Carbon Nanomaterials

Both graphene and CNTs have the potential to form LCs because their extreme aspect ratios give them mesogenic properties.[18,21] Since LLCs only occur above a critical concentration, sufficient dispersability can be difficult to achieve with graphene and CNTs, but due to their functionality GO and oCNTs are sufficiently dispersable and can achieve the nematic LC phase.[18,24] According to Onsager's hard-plate theory, a 2D particle, like a GO sheet, dispersion will form an LC at a certain volume fraction (Φ) as shown in the following equation:

$$\Phi \approx \frac{4T}{W}$$

where T is thickness and W is lateral width of a GO sheet.[24,29] Similarly, according to Onsager's rigid-rod theory, the critical weight fraction of oCNTs is given by the following equation:

$$weight\ fraction = \frac{3.3\rho d}{l}$$

where ρ is the density, d is the diameter, and l is the length of the tubes.[23]

GO and oCNTs form LCs but due to their differing shape, they align in different fashions. Confocal laser microscopy can be used to experimentally determine the orientational vectors of LCs as shown in Figure 7 for GO.[24] Since GO sheets are typically just one atom thick and can have micrometer scale lateral dimensions, they are essentially very thin discs.[25] Disc-like or oblate mesogens align along a discotic director that is perpendicular to the discs as shown in the model in Figure 7.[30] OCNTs also have a high aspect ratio, as their length is significantly larger than their diameter, even for shorter oCNTs.[18] So, oCNTs can be thought of as rigid rods, or prolate mesogens, that align along a calimitic director that is parallel to the rods as shown in Figure 4.[30] Mixtures of oCNT and GO LCs have not been previously reported but disc-rod LC combinations can be achieved if the disc-rod interactions are stronger than the rod-rod, and disc-disc interactions.[30]

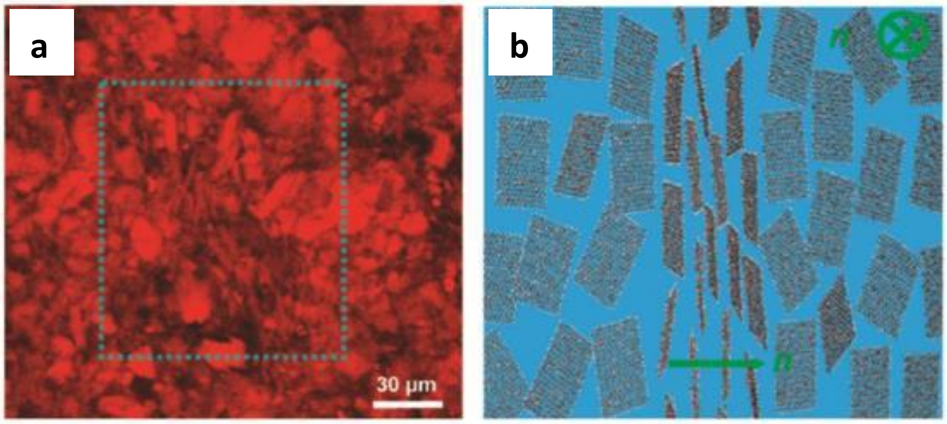

Figure 7. Laser confocal microscopy image of GO nematic LC (a) with a model showing the discotic director (b).[24]

Both GO and oCNT LCs have been used for the simple production of thin films via drop drying, and for the simple production of fibers via wet-spinning, but there are some challenges associated with working with LCs.[21,23] GO sheets have been shown to anchor homeotropically,or “face-on,” on liquid-air and liquid-glass interfaces.[29] GO can be thought of as having a hydrophobic basal plane and hydrophilic edges, so it's hydrophobic basal plan will interact with the air or glass causing the homeotropic anchoring.[29] As mentioned, surface anchoring can be a challenge when working with nematic LCs in channels, and because GO sheets have a very high surface area, they can form strong interactions with channel surfaces, which can lead to defects in the produced material.[28,29] OCNTs can vary greatly in length, which can have an impact on whether or not they can achieve the nematic LC phase.[31] If oCNTs are too short, their aspect ratio may not be large enough to drive the formation of the nematic LC phase, but if oCNTs are too long, even though their aspect ratio is high, entanglements can occur.[31] CNT length has been found to affect the orientational parameter (S), which according to Onsagers theory has a value of 0 for isotropic phases and a value of 0.79 for the isotropic to nematic transition.[31] Typically, this value is significantly lower than expected for oCNT LCs, but sonication can be used to shorten oCNTs and it has been found that S increases with increasing sonication time, implying that shorter oCNTs form nematic LCs with a greater degree of order.[31] Another challenge associated with both oCNTs and GO is that samples are likely to be polydisperse.[21,23] Figure 8 shows a phase diagram for LLCs including the so-called "Flory-chimney" or biphasic region.[23] This region will be more narrow for less polydisperse samples.[23] In the biphase, the particles with higher aspect ratios will preferentially enter the nematic LC phase, while particles with lower aspect ratios will remain in the isotropic phase.[23] So, separation of the isotropic and nematic phases enables the separation of particles based on their size.[23] In a study using oCNTs, repeated centrifuging of the biphase led to samples with smaller size distributions, and those samples displayed more narrow Flory chimneys.[23] A different study used the same technique to obtain a GO sample with a polydispersity of 13% compared to 83% from the crude sample.[21] Their improved GO LC was shown to have phase transitions close to the theoretical values.[21] Moreover, there may be some challenges in working with GO and oCNT LCs, but they are useful as a means to process novel carbon nanomaterials into ordered macroscopic structures.

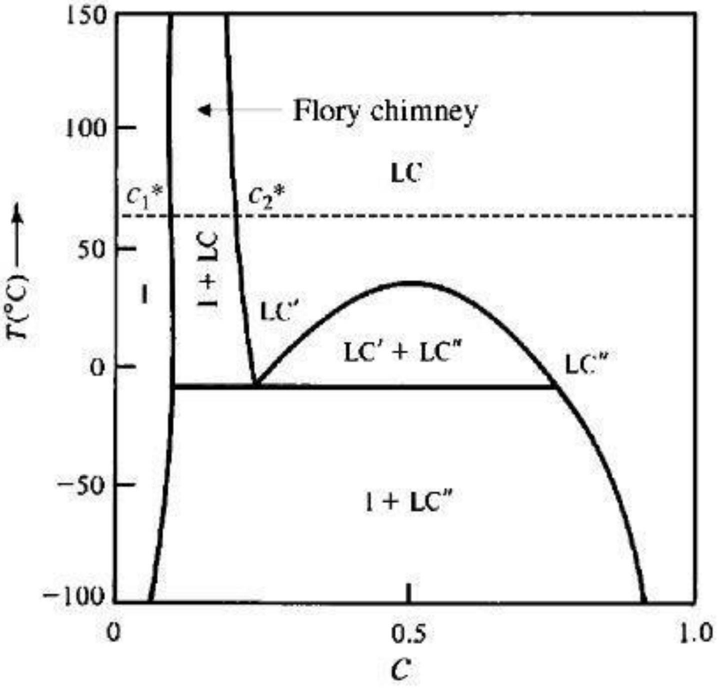

Figure 8. Phase transition diagram for nematic LLCs.[23]

1.3 High Performance Fibers

The first modern, high performance carbon fibers (CFs) were prepared in 1958 by Bacon, a physicist studying the triple point of graphite.[32] The graphite whiskers he discovered were shown to have a tensile strength of 20 GPa and a Young's modulus of 700 GPa.[32] Unfortunately, Bacon's method was neither cost-effective nor efficient.[32] In general, CFs are prepared via carbonization where carbon materials are heated to very high temperatures (1000-2500°C) to produce graphitic materials.[33] Only highly ordered precursors lead to graphitic crystalline structures with beneficial properties.[33] In 1964, Bacon and Schalamon used carbonization to prepare rayon based fibers, and used a novel "hot-stretching method" that helped to orient the graphite layers parallel to the fiber axis, thereby optimizing their mechanical properties.[32] These fibers had a Young's modulus of around 172 GPa, and were commercialized by Union Carbide under the trade name "Thornel 25."[32] Around the same time, Shindo prepared polyacrylonitrile (PAN)-based CFs that were highly oriented due to their pure PAN backbone, and were shown to have a Young's modulus of 140 GPa.[32] The British Royal Aircraft Establishment and Rolls Royce, Ltd. also investigated PAN-based CFs and were able to prepare fibers with strengths as high as 1.7 GPa and a modulus of 400 GPa.[32,33] This greatly contributed to the commercial boom of the CF industry in the 1970s.[32,33] Pitch, a tar-like substance consisting of carbon compounds with different branching and molecular weights, can also be used as a precursor for CFs.[32] Singer and Cherry used a "taffy-pulling" apparatus to apply stress to pitch in its LC phase, which significantly increased alignment, and was shown to result in fibers with a Young's modulus as high as 1 TPa.[32] As a reference, steel has a tensile strength between 1-2 GPa and a Young's modulus of 200 GPa, so it is clear to see that CFs have mechanical properties on par, or better, than steel with the added benefit of being lightweight, making them of great interest in a number of industries.[32] For the most part, pitch-based CFs are more expensive to produce and are used in more niche application such as aerospace.[32] PAN-based fibers are the most common commercial CF, and they are used in a variety of applications including sporting goods, automobiles, and aircrafts.[32] CFs have been shown to have novel, useful properties, and research in the field continues to drive down costs and open possibilities for more commercial applications.[32] But, a major limitation of carbonization techniques is the resulting polycrystalline graphitic structure, which includes large grain boundaries that significantly detract from the potential properties of CFs.[33] As mentioned, CNT and graphene have great promise as nanomaterial building blocks, and are excellent candidates for a bottom-up assembly technique to prepare fibers with properties that can compete with existing CFs.[33]

Graphene fibers (GFs) cannot be prepared via melt-spinning, due to graphene's incredible thermal stability, or via dry-spinning because graphene sheets do not form entanglements; so, wet-spinning is the only viable option for preparing GFs.[21] The wet-spinning dope is composed of a GO LC whose orientation can be controlled by the uniaxial flow leading to fibers with GO sheets aligned along the axis of the fiber.[34] The resulting gel-fiber is then deposited into a coagulation bath.[34] The coagulation bath must have favorable interactions with the GO LC solvent, but not with the GO sheets themselves.[34] For instance, Ca^{2+} in an EtOH/water mixture has been shown to be a useful coagulation bath for aqueous GO LC dopes, because the presence of an electrolyte disrupts the electrostatic repulsions that make GO dispersable.[34] When the produced GO fiber dries, it shrinks in the radial directions and a wrinkly texture can be observed due to GO sheets buckling.[34] The GO fibers can then be reduced to prepare neat GFs. Figure 9 shows the basic wet-spinning process and Figure 10 shows a more close-up look at the orientation of the GO sheets throughout the process.[33,34]

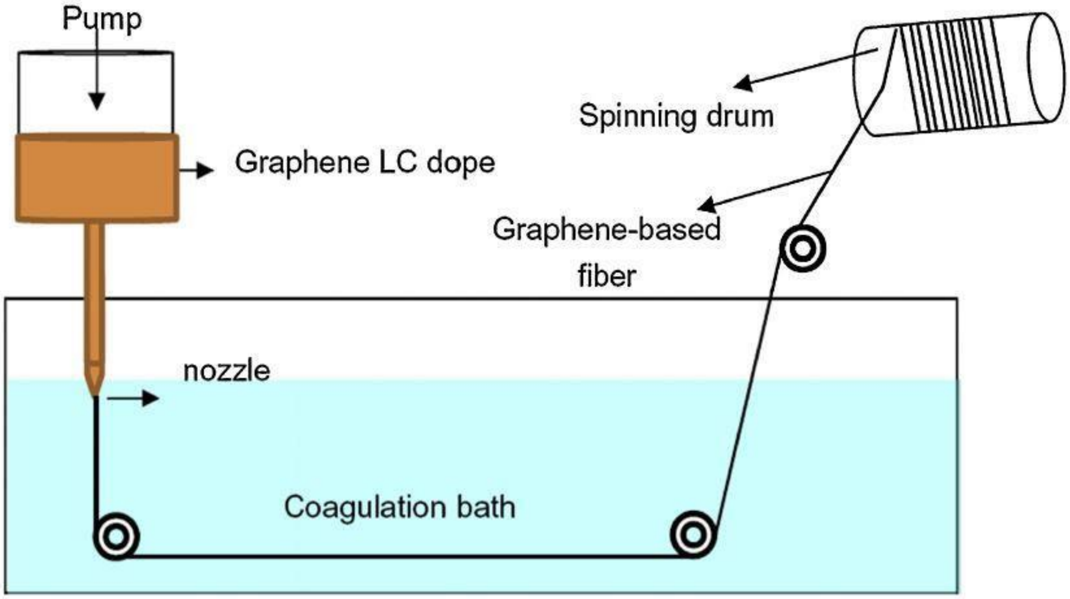

Figure 9. Schematic for the GO LC wet-spinning process.[33]

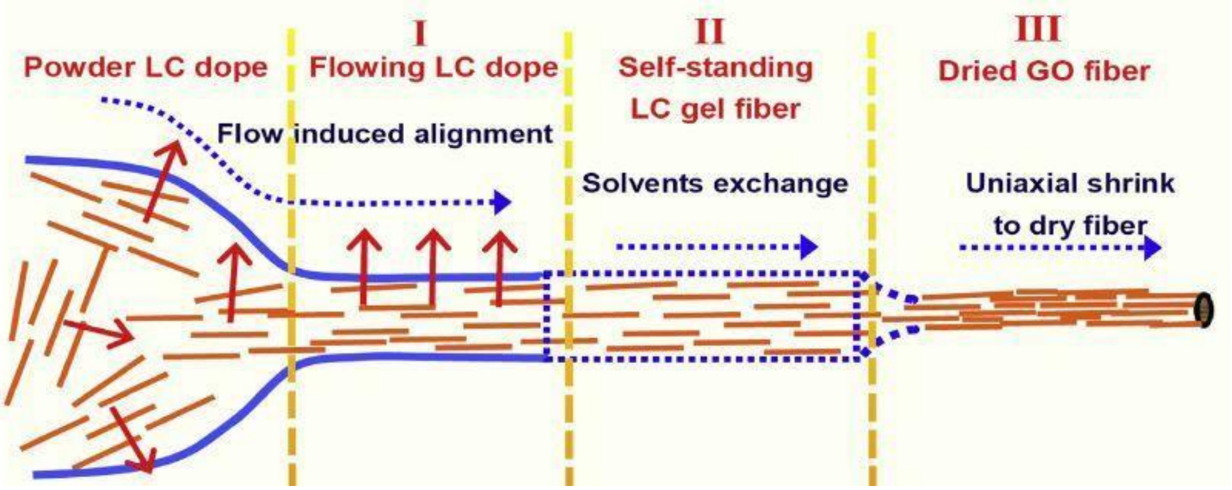

Figure 10. Effect of wet-spinning on GO sheet orientation.[34]

Xu & Gao have found a number of ways to optimize the properties of GFs prepared via wet-spinning of GO LCs. In one of their studies, the original polydispersity (PDI) of GO was about 83%, but size fractionation was used to reduce the PDI of the sample to around 13% leading to a more consistent GO LC dope.[21] Additionally, a very high concentration of around 5.7% (by vol.) GO was used in order to achieve the highly ordered, lamellar LC phase.[21] When lower concentration dopes were tested, they resulted in brittle fibers.[21] The results indicated that the diameter of the produced fibers varied from 50 to 100 μm and could be controlled by adjusting the size of the nozzle and changing the flow rate.[21] The resulting GO fibers had a tensile strength of 102 MPa, a Young's modulus of 5.4 GPa, and an elongation of 6.8-10.1%.[21] The flexible GO fibers were shown to undergo plastic deformation at room temperature due to the stretching and displacement of GO sheets.[21] Chemical reduction using 40% hydroiodic acid was used to produce rGO fibers with a tensile strength of 140 MPa, a Young's modulus of 7.7 GPa, and an elongation of 5.8%.[21] The higher strength observed in the rGO fibers can be explained by the more favorable interactions between rGO sheets and more compact stacking.[21] A few years later, the same team published another report where they investigated the effect of GO sheet size on fiber properties.[34] GO synthesis was tuned to produce GO sheets with tens of micron scale lateral dimensions, rather than the usual submicron dimensions.[34] The so-called giant GO sheets were used to prepare fibers using a coagulation bath containing Ca^{2+}.[34] The use of a divalent ion such as calcium introduces coordination cross-linking that strengthens the interlayer interactions between GO sheets, and results in fibers with more optimal mechanical properties.[34] Fibers produced with the so-called giant GO sheets in a Ca^{2+} coagulation bath were shown to have an increased strength of 412 MPa, which was further increased to 501 MPa following chemical reduction.[34] An alternative method was used by Dong *et al* where GFs were hydrothermally prepared by heating a glass pipeline used to confine a GO dispersion of 8 mg/mL.[35] These fibers were found to have a strength of 180 MPa, which was increased to 420 MPa following post-treatment annealing at 800°C.[35] The main focus of this work is optimizing mechanical properties, but it is worth noting that GFs can be multifunctional. For example, Dong *et al* introduced Fe_3O_4 nanoparticles into the GO dispersions to produce magnetic fibers.[35] Another note-worthy example is the production of moisture-controlled GO fiber rotary motors that were prepared by twisting GO LC fibers while still in their gel form.[36] The twisting treatment was also shown to optimize strength and flexibility of the fibers.[36]

CNT fibers can also be prepared via wet-spinning of LC dopes following along the same principles described in the above for GFs.[18] SWNT fibers were successfully prepared via wet-spinning an SWNT LC in H_2SO_4, and were reported to have good internal alignment and a Young's modulus of 120 GPa.[18] MWNT fibers were also successfully prepared via wet-spinning using ethylene glycol as the LC solvent.[18] Their modulus was determined to be 142 GPa, and the use of 1 mm long CNTs was thought to increase the contact area between the tubes resulting in enhanced tube-to-tube load transfer.[18] But, some literature suggests wet-spinning is not ideal for long CNTs, and high performance fibers have been reported using high quality 5 μm CNTs dispersed in chlorosulfonic acid.[37] The study noted that the fibers were collected on a drum that was set to have a velocity slightly higher than the spinneret exit in order to ensure stretching and high CNT alignment throughout the process.[37] The produced fibers had a tensile strength of 1.0 GPa, with a Young's modulus of 120 GPa, and an elongation of 1.4%.[37] Choice in solvent can also have a significant impact on fiber morphology depending on how quickly it evaporates.[18] When CNT fibers were prepared using ether, they were shown to have a collapsed structure and many voids, but when less volatile solvent like water or EtOH were used, the resulting CNT fibers were shown to have more uniform, circular cross-sections.[18] Another way to prepare CNT fibers via wet-spinning is to use a CNT polyelectrolye dispersion as the dope.[38] In a recent study, SWNT polyelectrolytes were stabilized with crown ethers in DMSO, and a concentration as high as 52 mg/mL, with LC behavior, was achieved.[38] SWNT fibers prepared using this method were shown to have a modulus of 14 GPa and a tensile strength of 124 MPa.[38] When the dope had a lower concentration of 9.4 mg/mL, the fibers were too brittle to be analyzed, but when the concentration of SWNTs was increased to 35 mg/mL, the strength was optimized.[38] One limitation is that sonication was used to increase dispersability, but this likely decreased the size of the CNTs and may have diminished some of the mechanical properties, but a benefit is that no superacids have to be used.[38] The SWNT polyelectrolyte study also used an NaI_3 coagulation bath that was shown to result in fibers with optimal conductivity, demonstrating the ease with which CNT fibers can be multifunctionalized.[38]

Another method that can be used to prepare CNT fibers is to solid-state spinning of bulk grown CNT arrays.[18] In general, this method has produced fibers with the best properties because long CNTs (0.5 to 1.5 mm) can easily be used with this method.[39] It is essential that the CNTs are well-aligned in the array, in order to prepare fibers with beneficial properties.[40] Fibers prepared from 1 mm long CNT arrays had a tensile strength of 1.35-3.3 GPa, a stiffness of 100-263 GPa, and a toughness of 975 J/g.[39] Other reports using a similar method have noted that the mechanical properties can be further improved by twisting the resulting CNT fibers with a reported strength of 1.9 GPa and a stiffness of 330 GPa.[41] One limitation with this method is that the resulting fibers usually have a low packing density, which detracts from the mechanical properties.[39]

A third way to produce CNT fibers is to directly draw fibers or yarns from CNT aerogels produced during CVD synthesis as shown in Figure 11.[42] Figure 11 depicts how lower concentrations of CNTs and higher flow rates can reduce entanglements allowing the aerogel fiber or yarn to be drawn at higher rates.[42] The fast drawing of the fiber or yarn allows the CNTs to be highly aligned with respect to the fiber axis.[42] Highly oriented CNT fibers produced using this method have a reported tensile strength of 1 GPa and a Young's modulus of 40 GPa.[42] Another report indicated CNT fibers with a maximum tensile strength of 1.46 GPa when hexane was used as the hydrocarbon source.[43] Lower results were achieved when EtOH and ethylene glycol were used, demonstrating the impact the CVD synthesis factors can have on the resulting CNT fibers.[43] Treatment with a volatile solvent achieves higher density of CNTs due to capillary forces.[41] Densification optimizes the stress transfer because it ensures that a greater proportion of CNTs will be fully load bearing.[41] CNT fibers densified in acetone were reported to have a specific stress five times greater than the as-drawn fibers.[41] EtOH has also been successfully used for densification of CNT aerogels and has also been shown to lock-in twists.[44] Twisted and densified fibers have been reported to have a toughness six times greater than only densified fibers.[41]

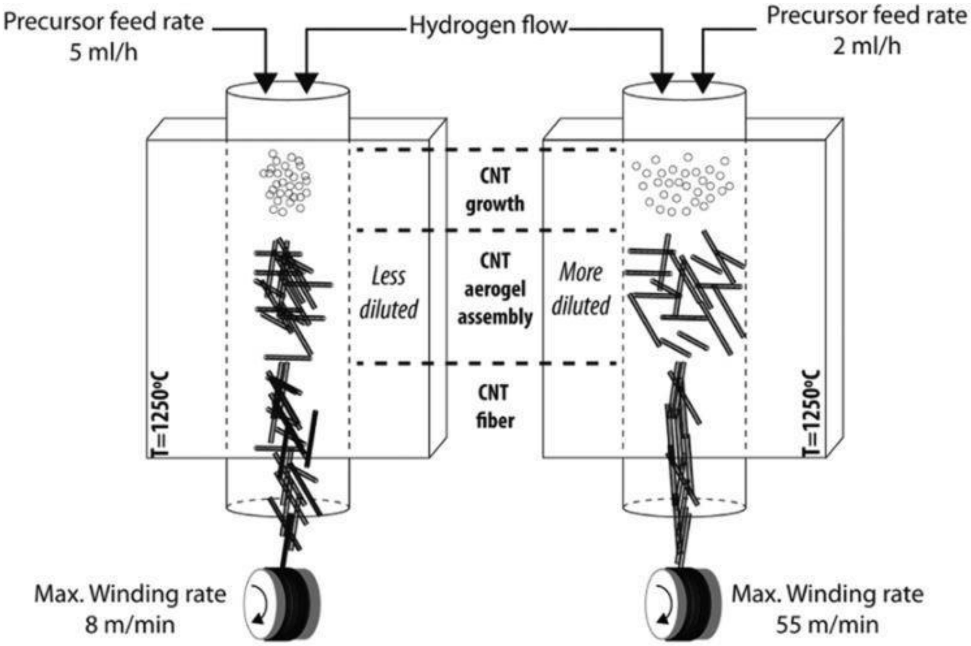

Figure 11. Schematic of the direct spinning process for CNT aerogels.[42]

Fibers prepared from materials besides graphene and CNTs have been shown to have improved mechanical properties with the addition of graphene or CNTs. Cellulose fibers were wet-spun, and with graphene loading as low as 0.2% (by wt), the fibers showed a 50% improvement in strength and a 25% improvement in Young's modulus.[5] The addition of both SWNTs and rGO flakes in a 1:1 ration, at 0.3% (by wt) each, was shown to have a synergistic toughening effect on poly (vinyl alcohol) PVA fibers.[45] Toughness is enhanced when nanoparticles that can interact favorably are introduced into polymer matrixes, because they allow for greater extension and better energy dissipation due to viscous sliding between nanoparticles.[45] Platelet shaped particles, like rGO flakes, have also been shown to be effective at crack deflection, because they increase the area of the crack and thereby reduce stress at the crack location.[45]

Both graphene and CNT based fibers have promising mechanical properties and their synergistic effects in other fibers suggest that hybrid graphene/CNT fibers will likely have more optimal properties. One study prepared hybrid fibers using CNT fibers drawn from CNT arrays that were soaked in GO nanosheets where the tensile strength was improved by 42 MPa.[46] This increase can be attributed to the GO sheets bridging non-neighboring CNTs allowing for additional load transfer.[46] Another study that prepared fibers in a similar manner noted that the tensile strength increased by 110 MPa after the addition of 0.025% (by wt.), which was further increased by another 20 MPa after reduction, because rGO interacts more favorably with CNTs.[47] These fibers were also noted to be able to be tied into knots with no obvious signs of fracture and to be able to be woven into common textiles due to their flexibility.[47] A more recent study used wet-spinning of GO LCs with dispersed few-walled CNTs (FWNTs).[48] When the CNT/GO ratio was lower than 1:3, the CNTs were shown to align in the axial direction.[48] Following reduction, the hybrid fibers were shown to have an increase in tensile strength of about 200 MPa.[48] All three of the studies also investigated electrical conductivity and determined that the combination of rGO and CNTs leads to more optimal electrical properties.[46-48] Hybrid rGO/CNT fibers are an excellent candidate for electrically conductive textiles, and have even been successfully fabricated into miniature energy devices as shown in Figure 12.[47]

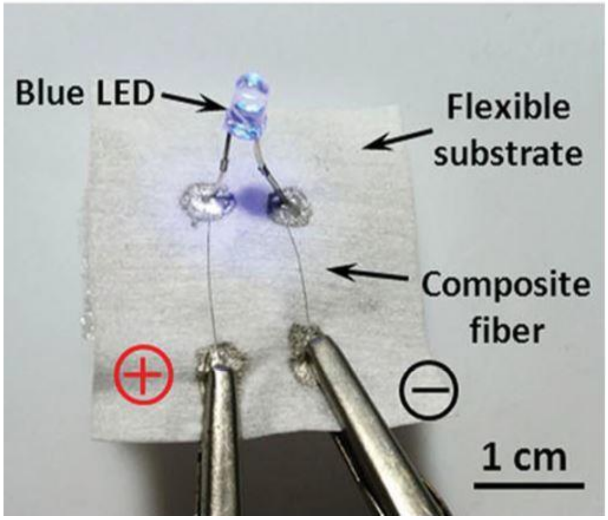

Figure 12. RGO/CNT hybrid fibers fabricated into an energy device.[47]

1.4 Research Plan

The purpose of this research is to develop a simple technique to prepare high performance, hybrid graphene/CNT fibers with enhanced mechanical properties. Dynamic mechanical analyses (DMA) will be used to analyze the mechanical properties of the fibers in conjunction with scanning electron microscopy (SEM), so that the mechanical data can be corrected based on fiber cross-section dimensions. Image processing programs can be used to determine fiber dimensions. The resulting fibers and their precursor materials can also be characterized in a number of ways using tools like spectroscopy and microscopy, in order to gain insight into their morphology and atomic structure.

The first method that will be investigated will use a CNT yarn drawn from an aerogel during CVD synthesis. Neat CNT fibers will be prepared by twisting strands of the yarn, and then densifying the fiber with a volatile solvent. Hybrid fibers will be prepared by soaking the CNT yarn strands in a GO dispersion prior to spinning and densification, which can be followed by reduction. This is a simple way to produce hybrid fibers, and the use of a CNT yarn produced via CVD and GO as precursors is relatively scalable and cost-effective.

The other technique for producing fibers will involve wet-spinning of LLCs using a microfluidic channel. GO and oCNTs will be synthesized and their LC properties will be characterized using POM. The flow rate, channel size, spinning dope, and coagulation baths are all variables that will be investigated to determine their effect on fiber morphology. Additionally, some of the fibers will be twisted and their properties will be compared to as-spun fibers. Using GO for wet-spinning has been shown to be successful in the past, and the addition of a microfluidic channel is expected to increase the alignment of the nanomaterials in the fiber.

2. Experiments and Methods

Graphene oxide was synthesized using a modified Hummers method resulting in an aqueous dispersion with a gel-like texture.[8] MWNTs were oxidized in a 3:1 mixture of H_2SO_4 and HNO_3 under ultrasonication resulting in an aqueous dispersion. Both products were attempted to be characterized using Fourier transform infrared spectroscopy (FT-IR), thermal gravimetric analysis (TGA), atomic force microscopy (AFM), Raman spectroscopy, POM, x-ray diffraction (XRD), and SEM. Two different methods were used to prepare hybrid fibers. GO LC dispersions were used to wet-spin fibers using a microfluidic channel, and oCNTs were mixed with GO LC dispersions in an effort to wet-spin hybrid fibers. In the second method, a CNT aerogel yarn was twisted and densified to prepare neat CNT fibers. The aerogel was also soaked in GO before twisting in order to prepare GO/CNT hybrid fibers that could be thermally reduced to rGO/CNT fibers. The fibers were primarily analyzed for their mechanical properties using DMA and for morphology using SEM.

2.1 Materials

All materials used in this thesis work were purchased from commercially available sources by Zhang's Research Group and were used as received. Graphite and KMnO4 were purchased from Sigma Aldrich. Concentrated HNO_3 (68-70%), and reagent grade EtOH (99.9%) were purchased from Akros Organics. Concentrated H_2SO_4, (98%), $Zn(NO_3)_2{*}6H_2O$, and $CaCl_2{*}2H_2O$ were purchased from Fischer Science. Multi-wall CNTs (MWNTs) (10-20 nm diameter, 10-30 µm length, >95 wt.% purity) were purchased from cheaptubes.com.

2.2 Graphene Oxide (GO) Synthesis

Graphene oxide (GO) was synthesized via a modified Hummers' method as shown in Figure 13. Concentrated H_2SO_4 (60 mL) and fuming HNO_3 (20 mL) were slowly combined in a 3:1 by volume ratio, beginning with dropwise additions of HNO_3 to H_2SO_4 in a 250 mL round bottom flask set in an ice bath. The mixture was allowed to stir for about 10 minutes and then graphite (2.00 g) was added to the r.b. flask, and the flask was removed from the ice bath. The mixture was left to stir at room temperature for 24 hours.

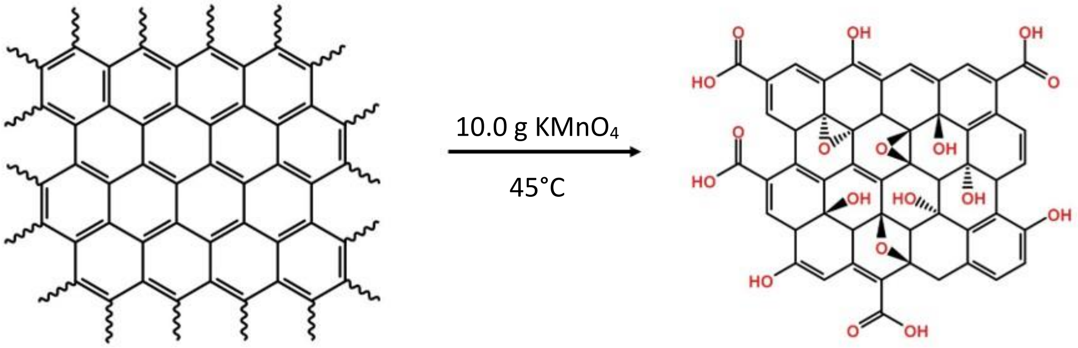

Figure 13. GO synthesis schematic.

The stirred mixture was poured into a 1000 mL beaker filled with DI water (~600 mL) and the beaker was set to stir. The precipitate was then vacuum filtered using microporous filter paper. The product was resuspended in DI water in a 500 mL r.b. flask. The flask was sonicated for about 20 minutes before being filtered again. This step was repeated a total of 4 times until the pH was about 5. The filter cake was dried in a glass petri dish at 70°C for 24 hours to obtain graphene intercalated compounds (GICs). Then, the GICs were heated to about 1025°C for 15 seconds in a furnace in order to obtain expanded graphite (EG).

The EG product was added to about 300 mL of concentrated H2SO4 in a 500 mL beaker, and the mixture was set to stir in an ice bath. Then, about 10 g of $KMnO_4$ was added slowly in order to maintain a moderate temperature no higher than 25°C. Once the mixture appeared to be stable and not in danger of over- heating, the mixture was set to stir in an oil bath set to 45°C. After stirring for about 4.5 hours, no distinct color change was visible, but, a slight viscosity increase was observed, so the reaction was quenched.

The reaction mixture was added to a 1000 mL beaker with DI water (~600 mL) in an ice bath. In the past, the water was added to the mixture but there were safety concerns because of the amount of heat produced. The current method used here was not shown to have any such problems. The reaction mixture was set to stir for about 30 minutes. Then, 6 mL of 30% hydrogen peroxide was slowly added to the reaction mixture in a dropwise fashion, in order to reduce any residual permanganate and manganese dioxide into soluble manganese sulfate. The original procedure directed the addition of about 6 mL; however, the amount added was around 12 mL until a color change to bright yellow was observed, at which point the reaction mixture was left to stir for about an hour.

The dispersion was transferred to 8 centrifuge tubes and they were centrifuged for 30 minutes at 17,000 RPM and the supernatant was removed. The GO was washed repeatedly with DI water followed by centrifugation until a pH of about 5 was reached. A vortex mixer was used to help redisperse the GO, and dispersability increased with the number of washes. To account for this change, higher RPMs of up to 25,000 were used. After about 12-15 washes, the samples from this quarter were determined to have a pH of about 5. The gel-like GO aqueous dispersion was combined from the centrifuge tubes and was used to prepare films on glass slides in triplicate, in order to determine the concentration.

2.3 Functionalization of Carbon Nanotubes (CNTs)

Multi-walled CNTs (MWNTs) were oxidized using a 3:1 by volume ration of concentrated H_2SO_4 (30 mL) and fuming HNO_3 (10 mL) according to Figure 14. The contents were placed in a 100 mL r.b. flask and they were placed in a bath sonicator at about 50°C for 20 hours. The sonicator does not have temperature control, so ice was used to make adjustments and while 50°C was the target, the actual temperature varied from 40°C to 60°C. Also, the sonicator only runs for 90 minutes at a time, so there were some instances where the reaction mixture was left outside of the sonicator, still in the acid mixture, at room temperature, overnight.

Then, the reaction was quenched in excess water in an ice bath. The dispersion was placed into 8 centrifuge tubes, which were spun at 17,000 RPM for about an hour and the supernatant was removed. The CNTs were attempted to be washed in a similar manner to the GO, but they were much more dispersable in water. So, after the initial centrifugation, very high RPMs up to 25,000 were used for as long as 3 hours at a time in order to achieve a pH of 4. A second batch was prepared using the same method but with a reaction time of 10 hours.

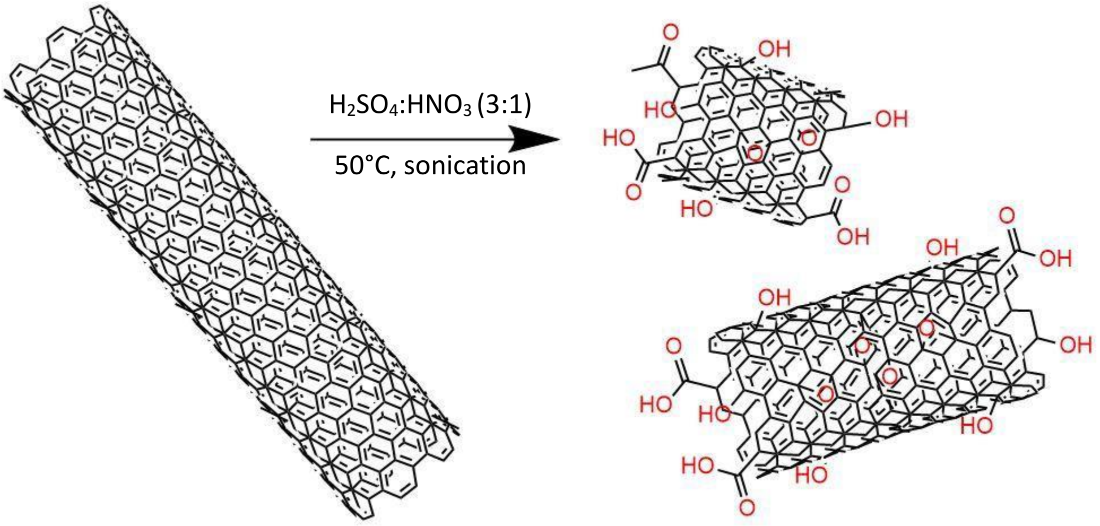

Figure 14. CNT functionalization schematic.

2.4 Fiber Preparation

2.4.1 CNT Aerogel-based Hybrid Fibers

A CNT yarn produced via CVD based aerogel spinning, as previously shown in Figure 11, was used as received from our collaborators at the IMDEA Materials Institute in Madrid. Neat CNT fibers were prepared by using thin strands of the CNT yarn, and twisting them with a motor, followed by densification with EtOH. In order to prepare hybrid GO/CNT fibers, thin strands of CNT yarn were soaked in a 0.18% (by wt.) aqueous GO dispersion prior to twisting and densification. In order to prepare rGO/CNT hybrid fibers, GO/CNT fibers were prepared followed by thermal reduction at 250°C for 24 hours in. Figure 15 shows how the hybrid fibers were prepared.

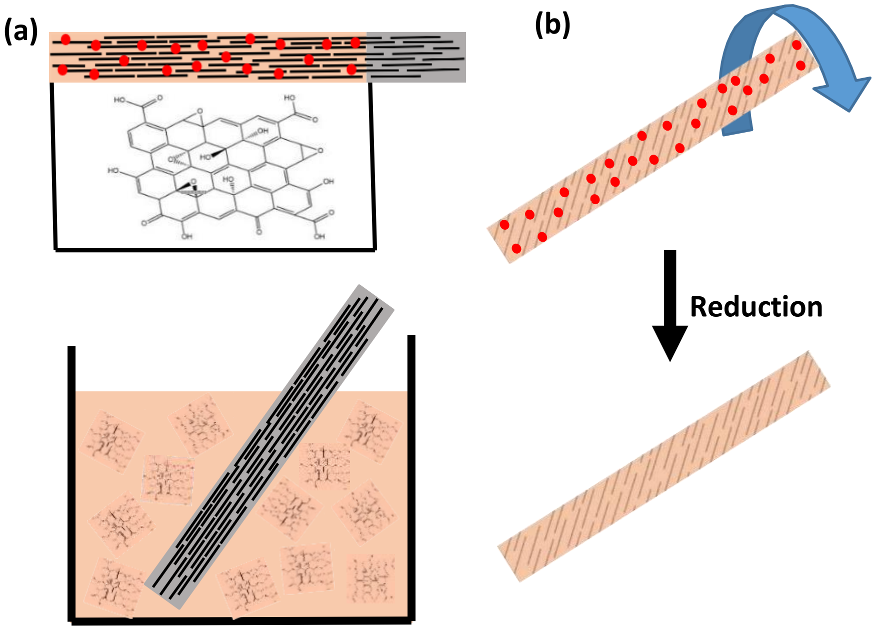

Figure 15. Preparation of CNT aerogel based hybrid fibers.

2.4.2 Microfluidic Spinning of GO LC Fibers

All fibers were prepared using custom poly (dimethyl siloxane) (PDMS) channels approximately 100 µm in height with varying channel widths. Polypropylene tubing with 0.5 mm diameter opening was used to connect the channel openings to a syringe pump to control the flow rate. Width of the channel, flow rate, type of GO LC dispersions, coagulation bath, and post modification steps like twisting, were varied. All fibers were dried across Teflon rods under IR light for about an hour, and were then allowed to air dry overnight. The basic set-up is shown in Figure 16.

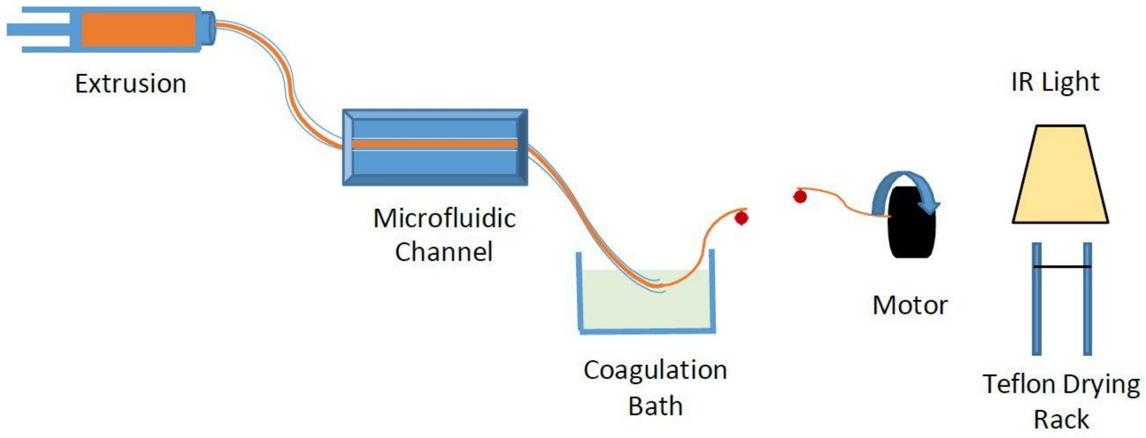

Figure 16. Microfluidic spinning process of GO LC fibers.

For the first comparison, a 75 µm X 100 µm channel was used, with a flow rate of 0.1 mL/hr and a 5% zinc nitrate ($Zn(NO_3)_2$) in isopropanol (IPA) coagulation bath. The GO dispersions were varied in concentration and solvent. The original GO product was diluted to 0.728% (by wt.) and 0.364% (by wt.), in either DI water, or in EtOH in order to compare a total of four different GO dispersions.

For the second comparison, a 0.364% (by wt.) aqueous GO dispersion was used at a flow rate of either 1 or 10 mL/hr in a 75 µm X 100 µm channel. Three different coagulation baths were used: a 5% $Zn(NO_3)_2$ in IPA solution, a 5% calcium chloride ($CaCl_2$) in EtOH solution, and a 5% $CaCl_2$ in IPA solution.

For the final comparison, a 0.364% (by wt) aqueous GO dispersion was used, with a 5% $CaCl_2$ in IPA coagulation bath at 5 different speeds ranging from 2.5 to 40 mL/hr. Four different channel widths were used: 50 µm, 75 µm, 100 µm, and 210 µm.

GO and oCNTs were combined in an attempt to create a dispersion that could be used to produce hybrid fibers. The oCNTs were centrifuged at 10,000 RPM for one hour, and the supernatant was used to dilute the original GO dispersion to ~0.46% (by wt). Sonication and mixing via vortexer were used in order to help disperse the oCNTs into the GO dispersion.

2.5 Characterization Techniques

FT-IR spectra was obtained using a Nicolet iS10 FT-IR spectrometer at a resolution of 16 cm^{-1} and with 1000 scans, in order to gain insight into the functionality of the synthesized products. Graphite powder, a GO film, and an rGO film were analyzed to verify the presence of oxygen-containing functional groups following oxidation, and the absence of oxygen-containing functional groups following thermal reduction. Similarly, IR spectra was obtained for pristine MWNTs and an oCNT film. GO and oCNT films were prepared via simple drop-drying onto a glass slide, followed by overnight drying in a desiccator. A GO film was thermally reduced to obtain a rGO film.

TGA was performed using a TA instruments Q500 with a heating rate of 10°C /min up to 550°C, after an isothermal step for 5 minutes. Films of GO, and rGO were analyzed in order to compare their decomposition. Labile oxygen-containing functional groups are expected to decompose around 200°C, so weight loss observed around this temperature indicates oxygen functionality, and its absence can be used to verify a successful reduction.[49]

AFM was performed using an Asylum MFP-3D-SA AFM. Dilute dispersions (~.01% by wt.) were prepared for GO and oCNTs, and they were drop dried onto a mica substrate. AFM used in conjunction with image analysis software such as Gwyddion can provide information about the size of the nanocarbon materials.

Additionally, the height can be analyzed in order to verify that individual sheets of GO have been produced. While AFM is a useful technique, instruments are known to have offsets as large as 0.5 nm due to various interactive forces, which can skew information for materials as thin as GO.[6] Graphene is expected to have a height of approximately 0.34 nm, and GO is expected to have a slightly larger height of anywhere from 1 to 1.4 nm due to oxygen functionality.[49]

SEM was performed using an FEI Quanta 200 microscope. All samples were secured to standard mounts using carbon tape. All samples were gold sputtered for at least 30 seconds. Dilute dispersions (~0.01% by wt.) were prepared for GO and oCNTs that were drop dried onto silicon wafers or mica in an attempt to determine their average size. Fibers were also imaged in order to determine their morphology. Some fibers were secured to 45° angled specimen holders in order to analyze their cross-section following mechanical analyses.

Optical reflection microscopy was performed on a Leica DM 2500 P polarized optical microscope (POM). This method has been used in previous studies as a more facile method, compared to AFM or Raman, for obtaining information about the size of graphene layers.[50] Dilute GO dispersions (~0.01% by wt.) were drop dried onto silicon wafers in an attempt to gain insight about the shape and size of individual GO sheets. GO/oCNT dispersions were also analyzed using this method as a way to check for aggregates.

XRD was performed using a Siemens Diffractometer D5000 using a rate of 1 deg/min with a 0.1 increment. Graphite powder, a GO film and an rGO film were prepared using the same techniques used for previous characterization methods. XRD is a useful technique, in that, it provides information about a materials crystalline structure.[51] Values are obtained for 2 theta (2θ), which can be used to calculate the d-spacing of a material according to Bragg's Law:

$$n\lambda = 2dsin(\theta)$$

where λ is the wavelength of the x-ray, θ is the Bragg angle between incident rays and the surface of the samples, d is the spacing between atoms in the sample, and n is an integer value where constructive interference occurs.[51] Based on previous reports, pristine graphene is expected to have a d-spacing of 3.4 Å, which should increase to around 7.8 Å for GO due to oxygen functionality.[14] Theoretically, rGO should have a d-spacing that matches that of pristine graphene, but typically the observed peak is much broader for rGO than it is for graphene due to defects.[14]

POM was performed using a Leica 2500 P microscope. Various dilutions were prepared using the original GO dispersion in order to determine the isotropic to biphase (I-B) and biphase to nematic (B-N) LC phase transitions for the prepared GO. The GO/oCNT mixtures were also analyzed using POM in order to ensure that the oCNTs had been successfully combined with the GO without disrupting the GO LC. POM was also used to analyze the texture of the GO LC as it was pumped through the microfluidic channels.

Raman spectroscopy was performed using a Thermo Scientific DXR Smart Raman with an excitation wavelength of 780 nm. Carbon-carbon double bonds lead to high intensity when using Raman, so this can be a useful tool for analyzing carbonaceous materials.[52] Two major peaks can be used to determine the relative degree of functionalization: the D band at around 1330 cm^{-1} correlates to disordered graphite materials, and the G band at around 1590 cm^{-1} correlates to ordered carbon.[20] So, the D:G ratio can be utilized to determine the relative degree of functionalization or defects.[52]

DMA was performed using a TA instruments Q 800. All fiber samples were analyzed using 20 mm paper frames. Force ramps were used with varying rates, depending on the fibers being tested, in order to obtain stress strain curves. DMA data was corrected using the static force divided by the cross sectional area, which was estimated using SEM images and ImageJ software. Stress-strain curves were used to determine various mechanical properties of the fibers including Young’s modulus, tensile strength, elongation, and toughness.

3. Results and Discussion

3.1 Characterization of Synthesized Products

The synthesized products were characterized using a number of techniques. The functionality of the products can be compared to the starting materials using FT-IR as shown in Figure 17 and 18.

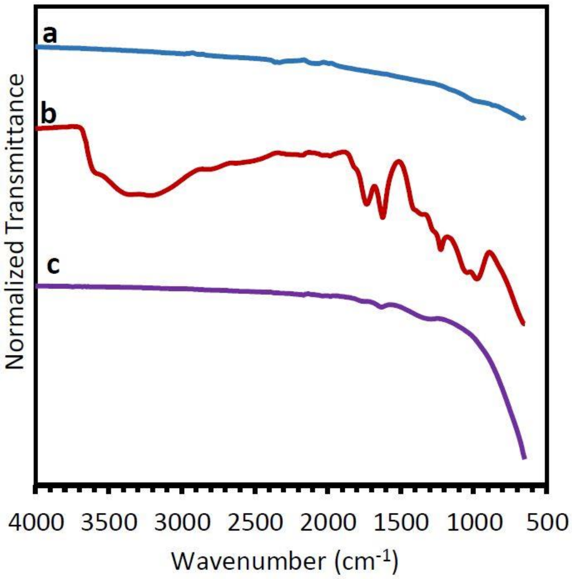

Figure 17. FT-IR spectra for graphite (a), GO (b), and rGO (c).

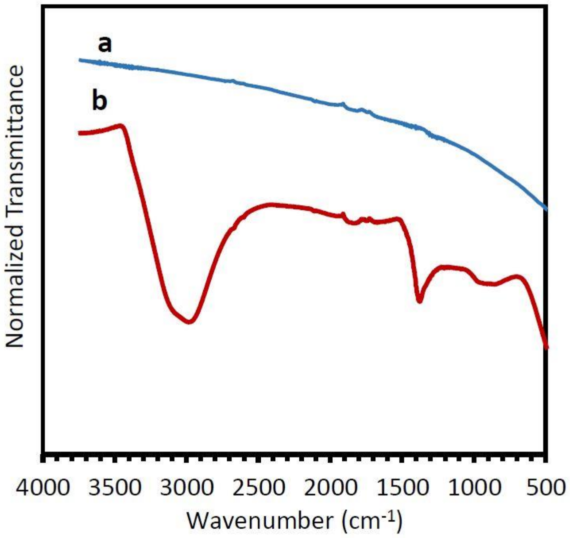

Figure 18. FT-IR spectra of pristine MWNTs (a) and oCNTs (b).

As shown in Figure 17, peaks associated with oxygen functionality appear after oxidation, and then disappear following thermal reduction. The broad peak from 3000-3500 cm^{-1} is caused by O-H bond stretching. While this could be associated with alcohol or carboxylic acid groups, it can also be caused by absorbed water. The peak around 1730 cm^{-1} is associated with C=O stretching and may be indicative of ketone or carboxylic acid functionality. The peak around 1680 cm^{-1} is associated with C=C stretching. The remaining peaks at around 1220 cm^{-1} and near 1000 cm^{-1} are likely associated with C-O stretching and indicate the possible presence of alcohol, carboxylic acid, or ether groups. The FT-IR data suggests possible oxygen-containing functional groups of GO, and verifies that the thermal reduction was successful. In Figure 18, the pristine MWNTs do not show any significant peaks implying their lack of functionality. The oCNTs have a broad peak between 3000 and 3500 cm^{-1} suggesting the presence of OH groups, and a peak around 1620 cm^{-1}, which is representative of aromatic C=C stretching. There is also a broad peak somewhat close to 1020 cm^{-1}, which could beassociated with a C-O stretch. There is no presence of a C=O stretch suggesting that the functional groups present on the oCNTs are likely alcohols or ethers.

SEM, AFM, and reflection microscopy were used in an attempt to gain insight into the size of the synthesized products. Figure 19 shows oCNTs drop dried onto silica whose size was determine to be around 200-300 nm using ImageJ software. The intended size was 0.5 to 1 µm, so a new batch was synthesized using a 10 hour reaction time as opposed to a 20 hour reaction time. Images could not be obtained for the new batch, but based on their high dispersability in water, and the difficulty in obtaining SEM images of the oCNTs, they still may have been too small in size due toover-oxidation.

Previous literature suggests the reaction conditions used should produce functionalized CNTs in the desired length range, but commercial sources are often highly impure, which may explain why both batches appeared to be over oxidized.

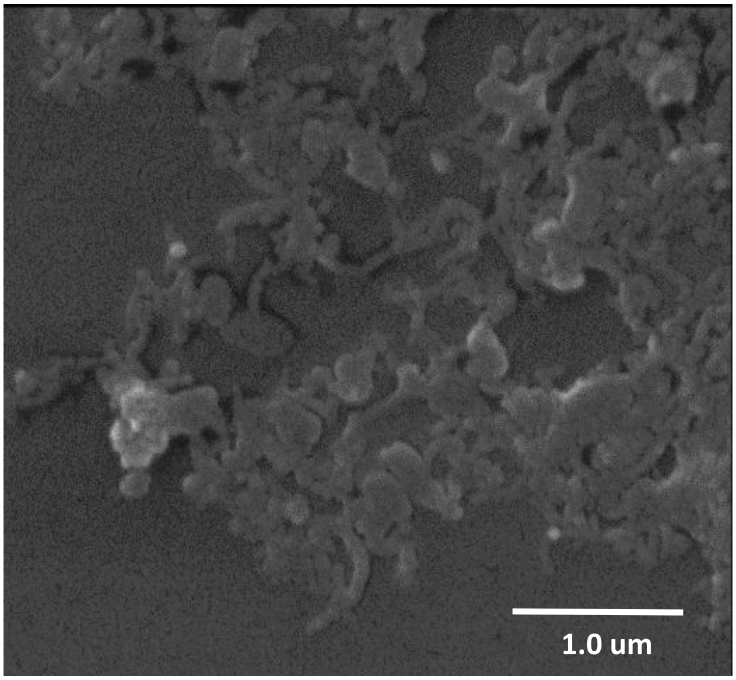

Figure 19. SEM image of the 20 hour batch of oCNTs.

SEM images were also obtained for the GO drop dried onto mica as shown in Figure 20. Even though individual sheets were not visible, the shriveled appearance and irregular shape of the GO suggests it may also be over-oxidized leading to some defects in its structure. The Hummers' method procedure suggests oxidizing until a color change from green to a different shade of green is visible, accompanied by an increase in viscosity. This change was not observed until about 4.5 hours. A new batch of GO was eventually synthesized using a predetermined time of 3.5 hours.

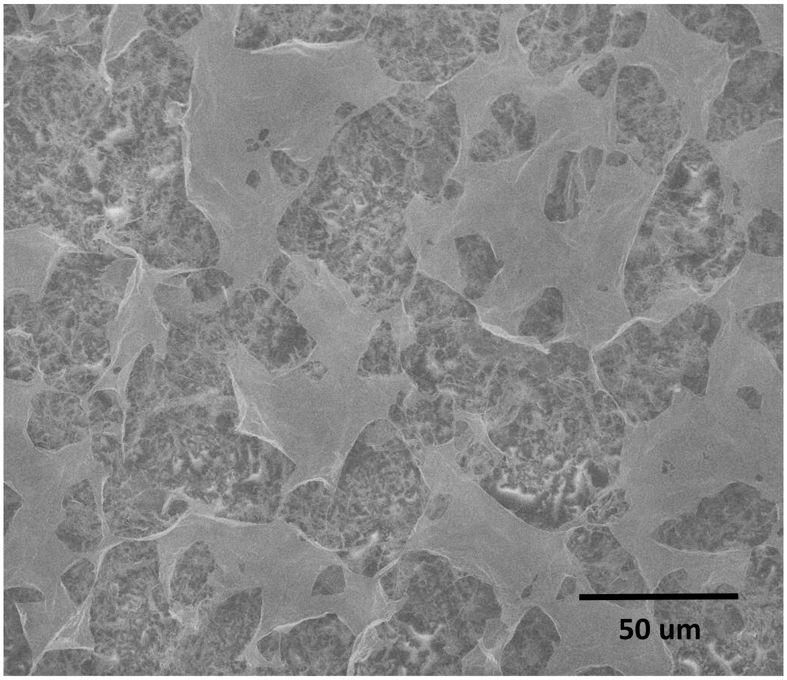

Figure 20. SEM image of the 4.5 hour batch of GO.

Two AFM images of GO drop dried onto mica are shown in Figure 21. In Figure 21 a, the irregular shaped clusters of GO sheets are visible. Obtaining images of individual sheets is difficult because the GO sheets often dry in aggregates. In Figure 21 b, what looks similar to a GO sheet can be seen in the middle of the image, but when it's height was determined with Gwyddion imaging software, it was shown to be between 1.8 and 2.0 nm in height. Pristine graphene is typically around 0.34 nm in height while GO has been reported to be anywhere from 1.0 to 1.4 nm in height due to the added functionality.[14] Considering the observed height was higher than what was reported in previous literature, there might be errors in AFM height values, which can be as great as 0.5 nm, or this region may actually include a few GO sheets.[6] Also, the substrate chosen was mica because its hydrophilicity should help the GO spread out and improve the chances of finding individual sheets, but its surface height varies, which can also lead to errors when obtaining height data via AFM. AFM images were also attempted for the oCNTs, but none of the images came out with a high enough resolution, and there were often AFM artifacts in the images obtained. So, another technique combining AFM with scanning tunneling microscopy (STM) was used and some images were obtained for the 10 hour batch of oCNTs as shown in Figure 22. Figure 22 a shows what is likely an aggregate of oCNTs, and Figure 22 b shows what is believed to be an individual oCNT. In both images, some AFM artifacts are visible. The individual oCNT was determined to be about 220 nm, using Gwyddion imaging software, similar to the SEM results for the 20 hour batch. However, in order to determine the average size of all of the oCNTS, many more images of individual oCNTs would be required. One challenge in working with MWNTs is that their diameter is variable so it is difficult to verify if the oCNT is isolated. When SWNTs are imaged their diameter can be measure to ensure there is only one oCNT present.

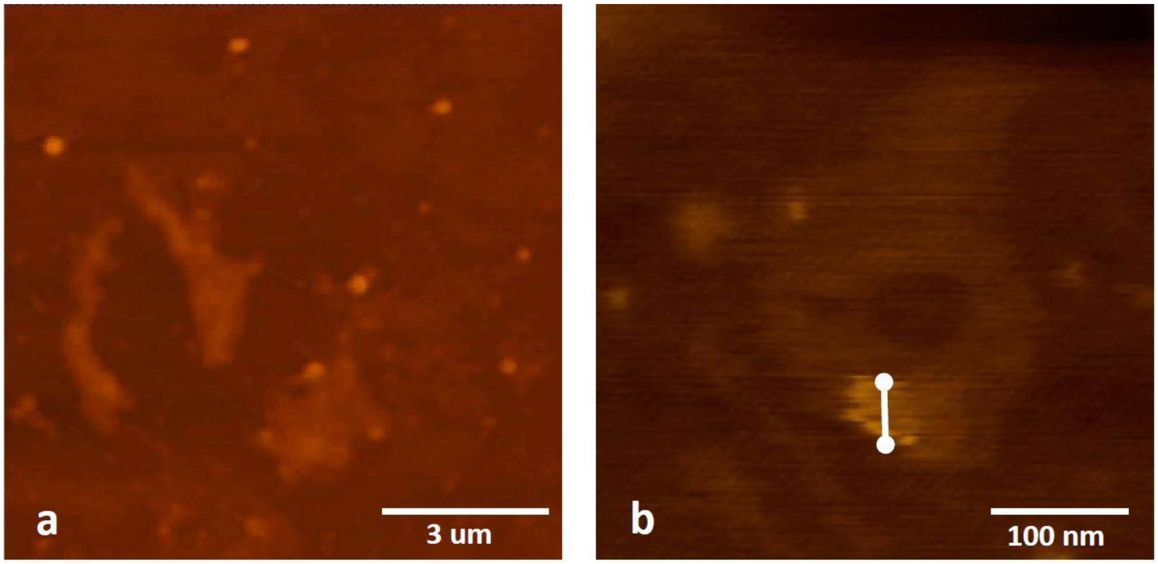

Figure 21. AFM images showing GO aggregates (a), and a few sheets of GO (b).

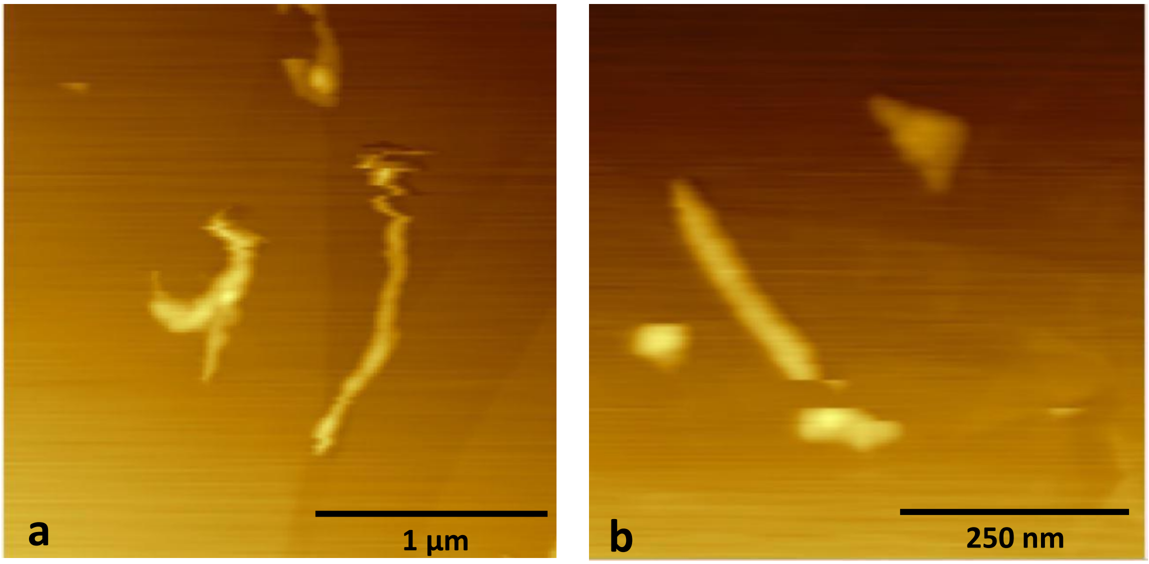

Figure 22. AFM-STM images of oCNT aggregates (a), and an individual oCNT (b).

The last imaging technique used was optical reflection microscopy for a sample of GO sheets drop dried onto silica wafers, as shown in Figure 23. This shows what is likely an aggregate of GO sheets. There are varying levels of contrast within the region that contains GO; the regions with higher contrast represent regions with more layers of GO sheets. Additionally, the aggregate was measured to be approximately 9 X 25 µm using Image J software, which is too large of a size to indicate a singular sheet. In previous literature, GO sheets produced using a very similar method had a mean size of only ~5.0 µm.[22] To effectively use this technique to identify singular GO sheets based on contrast measurements from optical reflectance images, a more powerful lens would be necessary.

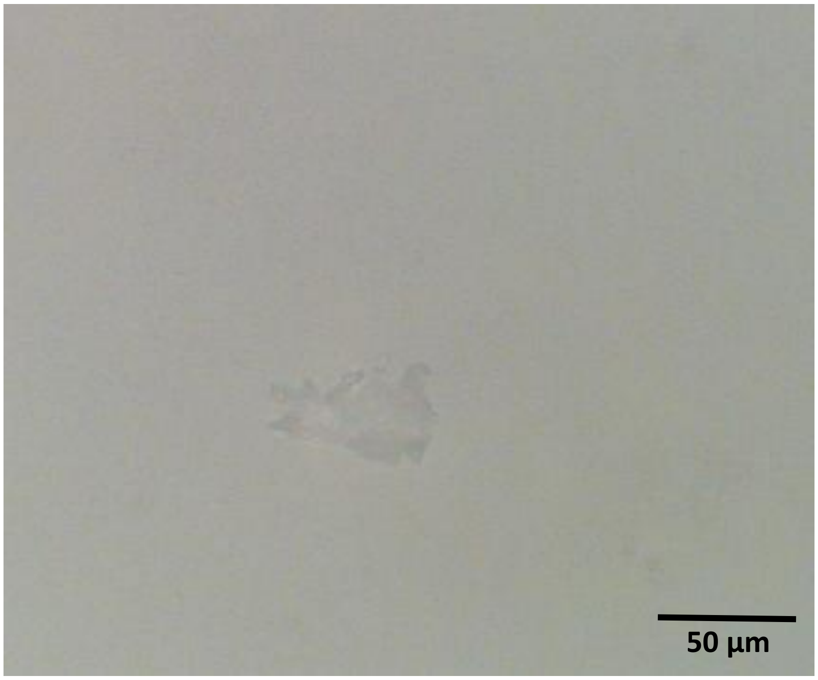

Figure 23. Optical reflectance image of several GO sheets.

Raman spectroscopy can be especially useful for carbon-based materials because while IR requires bonds with a dipole, Raman simply requires that the bonds be polarizable, so Raman can offer meaningful information about carbon-based materials like graphene and CNTs. As mentioned previously, the G band, typically found near 1575 cm^{-1}, is a signal for sp^2 carbons, while the D band, typically found near 1355 cm^{-1}, is a forbidden transition for sp^2 carbons, so it only appears in the presence of defects. The D:G ratio displays the relative amount of defects in the carbon nanomaterials. Figure 24 shows the Raman spectra for GO films, and for a thermally reduced GO film.

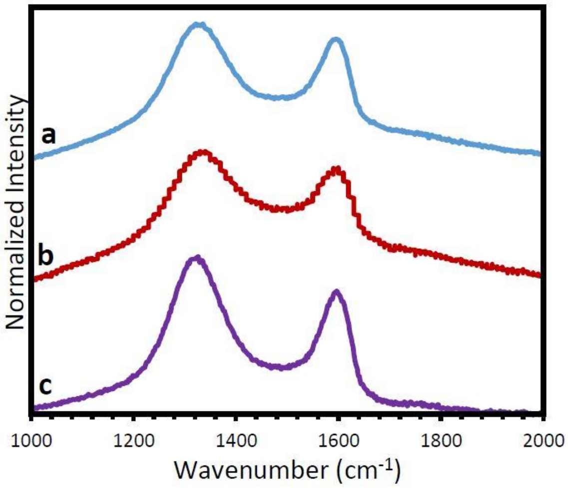

Figure 24. Raman spectra for a GO film from the 4.5 hours batch (a), a GO film from the 3.5 hour batch (b), and an rGO film (c).

The D band exists around 1330 cm^{-1} and the G band exists around 1600 cm^{-1} for all of the samples, which is slightly different than the reported literature values, but this can be attributed to a difference in wavelength in the Raman spectrometer used in this work. The D:G ratios are 1.12, 1.11, and 1.29 for the 4.5 hour GO film, the 3.5 hour GO film, and the rGO film respectively. The newer batch of GO, oxidized for less time, has a similar D:G ratio as the 4.5 hour GO film. This implies that their degree of functionalization is likely similar and that problems with the 4.5 hour batch are more likely due to smaller sized GO sheets. Ideally, after reduction the number of defects would decrease as the sp^3 functionalized carbons returned to the sp^2 structure of pristine graphene, but here the D:G ratio for rGO is greater than it is for GO showing how the high temperature used in reduction can lead to high pressures that result in even more defects following reduction. This explains why rGO typically displays less optimal properties than pristine graphene.

XRD is a useful technique for determining the d-spacing of crystalline materials. The XRD plots for graphite, GO, and rGO are shown in Figure 25. Based on the 2θ peaks, the d-spacing was determined to be 3.4 and 8.2 Å for graphite and GO respectively. This is consistent with reported literature values. However, for rGO, the peak is expected to shift back to around 26°, but in literature is usually reported as a broad peak, rather than a narrow peak as shown with graphite. Here, the rGO curve does not have a peak in this region, and only has a faint, and very broad peak, near 13.8°, which correlated to a d-spacing of 6.4 Å. This suggests there may be remaining functional groups, or that the crystalline structure is imperfect following thermal reduction.

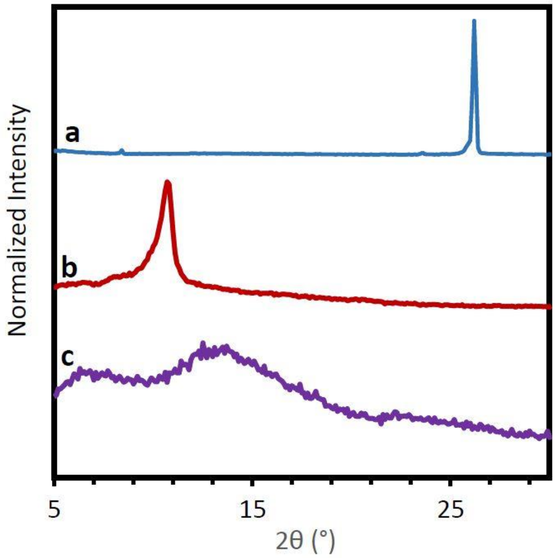

Figure 25. XRD spectra for graphite (a), GO (b), and rGO (c).

TGA data can also provide useful information about the presence of functional groups, because oxygen functionalities will degrade around 200°C. The TGA traces for GO and rGO are shown in Figure 26. GO undergoes three mass losses. The first of about 20%, at about 100°C, is caused by water absorbed in the film, while the second mass loss of about 37%, at about 200°C, is caused by the loss of oxygen- containing groups. The rGO was only shown to undergo one mass loss at a temperature near 500°C. These results confirm the presence of oxygen functionality in the GO and suggests the complete absence of any functionality in the rGO. This illustrates a possible benefit of using thermal reduction, in that, it does appear to completely reduce the GO.

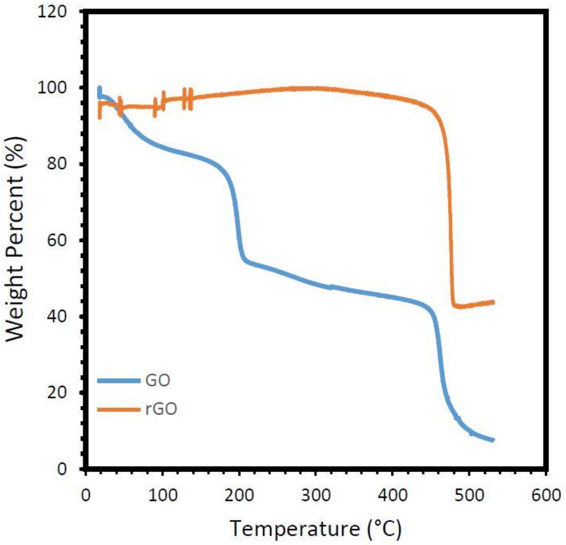

Figure 26. TGA traces for GO and rGO.

POM can also provide insight into the synthesized GO based on the observed LC textures. As mentioned, the original batch of GO used in this work was thought to have been over-oxidized. Figure 27 shows two POM images depicting disclinations in the GO LC. Additionally, Figure 28 shows a side by side comparison of the LC texture observed in the 4.5 hour batch and the 3.5 hour batch. The 3.5 hour batch has a more well-defined Schlieren, or brush-like, texture, and did not appear to have as large of disclinations as the 4.5 hour batch. Based on the POM images, the 3.5 hour batch of GO is of higher quality than the 4.5 hour batch.

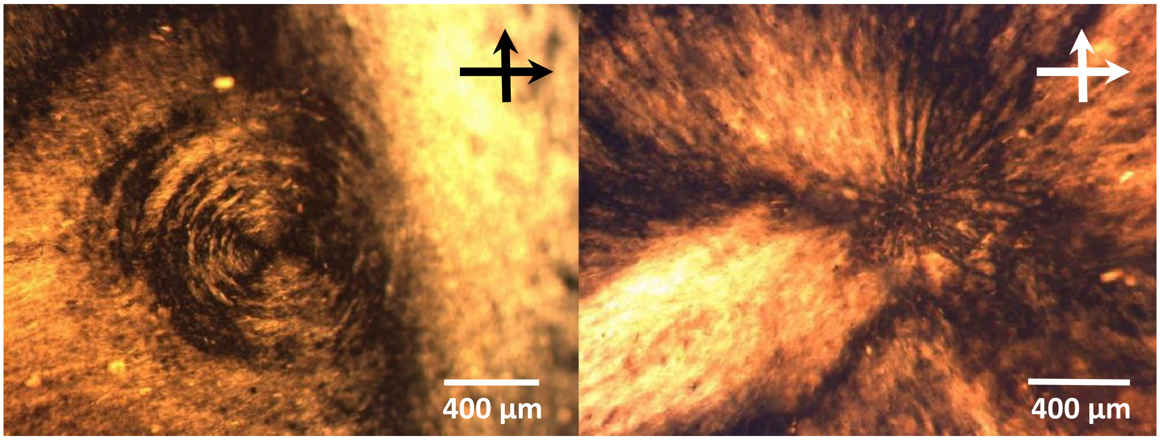

Figure 27. Examples of S=+1 disclinations observed in the 4.5 hour GO batch.

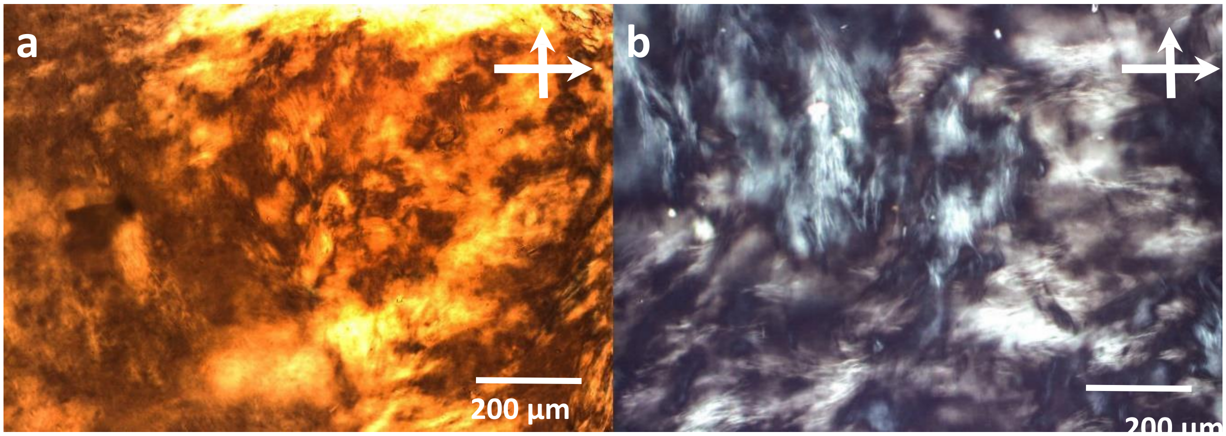

Figure 28. GO LC texture for the 4.5 hour batch (a) and the 3.5 hours batch (b).

3.2 CNT Aerogel-based Hybrid Fibers

Three types of fibers- neat CNT, CNT/GO, and CNT/rGO fibers were prepared and analyzed via Raman spectroscopy for characterization, via SEM to determine morphology, and via DMA to determine their mechanical properties. The Raman spectra for the three types of fibers is shown in Figure 29.

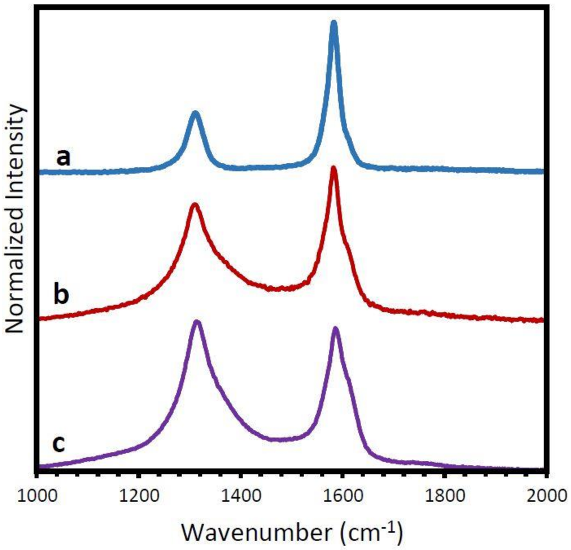

Figure 29. Raman spectra of neat CNT fiber (a), CNT/GO fiber (b), and CNT/rGO fiber (c).

The D:G ratio was determined to be 0.394, 0.744, and 1.08 for the neat CNT fibers, the CNT/GO fibers and the CNT/rGO fibers respectively. The determined D:G ratio for the neat CNT fibers is relatively low for MWNTs, so this is an indication that the starting CNT aerogel yarn material does not contain a large number of defects. The D:G ratio increases for the CNT/GO fiber due to added oxygen functionality. Note that this value is between the D:G ratio of the neat CNT fibers, and the previously determined value for the GO film. This is reasonable because the area analyzed may include regions mostly covered by a GO film but with the CNT yarn still present. Similarly, the D:G ratio for the rGO/CNT fiber falls in between the D:G values obtained for the neat CNT fibers and for the rGO film. Again, the rGO samples have the highest D:G ratio implying that the thermal reduction may actually increase the number of defects compared to the GO samples. SEM images to observe fiber morphology are shown in Figure 30.

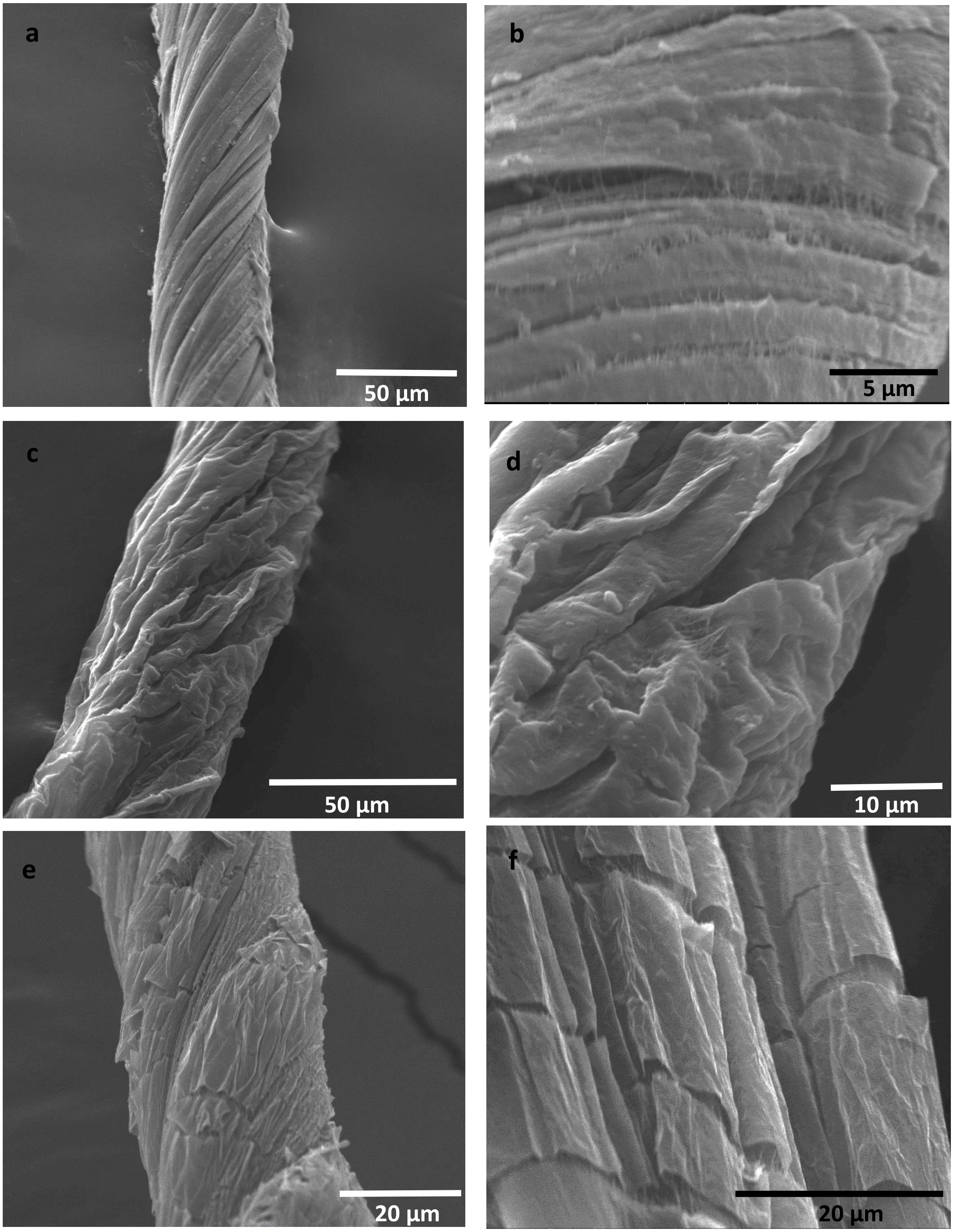

Figure 30. SEM images for the neat CNT fibers (a) & (b), the CNT/GO fibers (c) & (d), and the CNT/rGO fibers (e) & (f).

Figure 30 (a), (c), and (e) confirm that all three types of fibers are sufficiently twisted. The close-up morphology in Figure 30 (b), (d), and (f) shows visible CNT fibrils for the neat CNT fibers, and characteristic wrinkling for the CNT/GO and CNT/rGO fibers. When the GO sheets dry, they buckle to produce a wrinkled texture. This texture includes cracking in the CNT/rGO fiber suggesting the thermal reduction may cause some damage to the rGO structure. A total of 14, 18, and 17 trials were performed for the neat CNT, CNT/GO, and CNT/rGO fibers respectively. The SEM images for each type of fiber were analyzed visually to ensure that all hybrid fibers included the GO or rGO sheets as confirmed by wrinkled texture. If the wrinkled texture was not observed, the fibers were removed from the data set. Another variable that was examined was the twist angle. Only fibers with a twist angle between 20 and 50° were kept in the sample, so that fibers that had not been sufficiently twisted were also removed from the data set. Two of the fibers in this range displayed novel fracture morphology for the CNT only fibers. Based on previous literature, these two fibers had been twisted and densified in such a way that their mechanical properties were altered, so these two fibers were also removed from the data. In the end, at least seven trials were kept for each type of fiber. Stress-strain curves were determined using DMA and representative curves are shown in Figure 31. Table 1 also summarizes the mechanical properties for each type of fiber, and Figure 32 shows the trends in mechanical properties for each type of fiber.

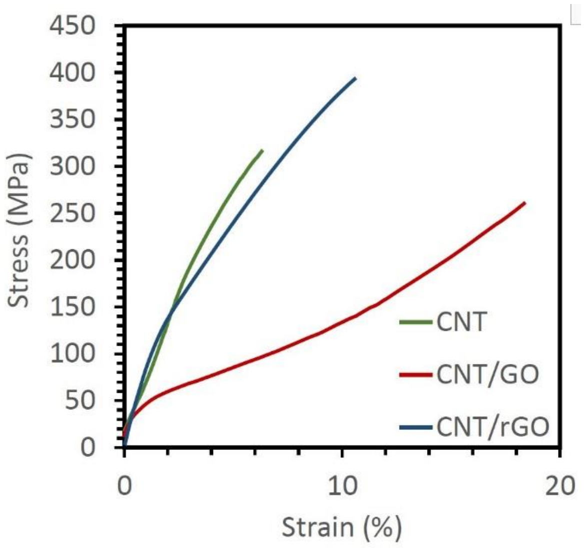

Figure 31. Representative stress-strain curves for the three types of CNT aerogel-based fibers.

Table 1. Summary of average mechanical properties for the CNT aerogel-based fibers.

Type of Fiber	Tensile Strength (Mpa)	Modulus (Gpa)	Elongation (%)	Toughness (J/g)
CNT	327	9.10	7.55	13.43
CNT/GO	232	3.82	19.1	21.6
CNT/rGO	388	9.83	9.90	23.5

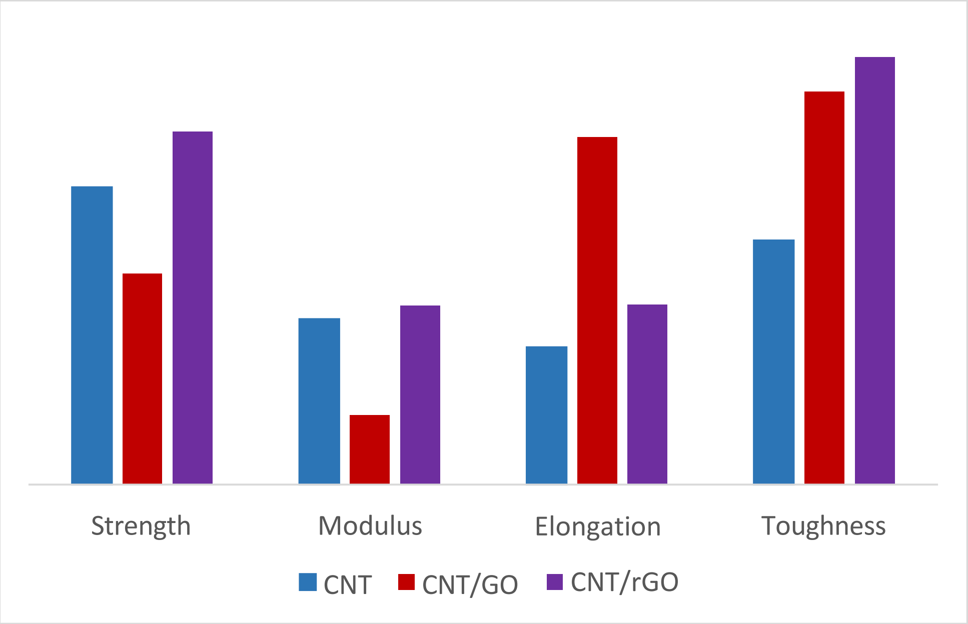

Figure 32. Trends in mechanical properties of the CNT aerogel-based fibers.

The stress strain curves obtained in Figure 31 were collected using a force ramp rate of 0.015 N/min. Then, the static force was divided by the cross-sectional area. The cross-sections were all assumed to be circular, and their diameter was determined with SEM images and Image J software. For each fiber, three images were taken of different parts of the fiber and five measurements were made for each of the three images resulting in sample sizes of 15 measurements. The representative curves show that the neat CNT and CNT/rGO stress-strain curves have similar shapes, and similar properties, except the CNT/rGO has more optimal properties. The CNT/GO curve has a different shape with a larger strain-hardening region. While the strength and modulus decreased for the CNT/GO fibers, compared to the neat CNT fibers, the elongation increased by a significant amount and toughness increased. Essentially, both types of hybrid fibers achieved a more optimal toughness but via different mechanisms. The rGO/CNT fibers achieved greater toughness by optimizing tensile strength while the GO/CNT fibers achieved greater toughness by optimizing elongation. The GO and CNT aerogel do not have favorable interactions, but GO can still be incorporated into the fiber as verified in Figure 30 (c) & (d). The presence of GO sheets allows for contact between non-neighboring CNT rods, and allows for more sliding, thereby increasing the fibers flexibility, or elongation. For the rGO and CNT combination the interactions between rGO sheets and CNTs is favorable, so the increased contact between non-neighboring CNTs leads to an increased load transfer allowing for a greater strength to be achieved. A model is shown in Figure 33 to visualize this phenomenon.

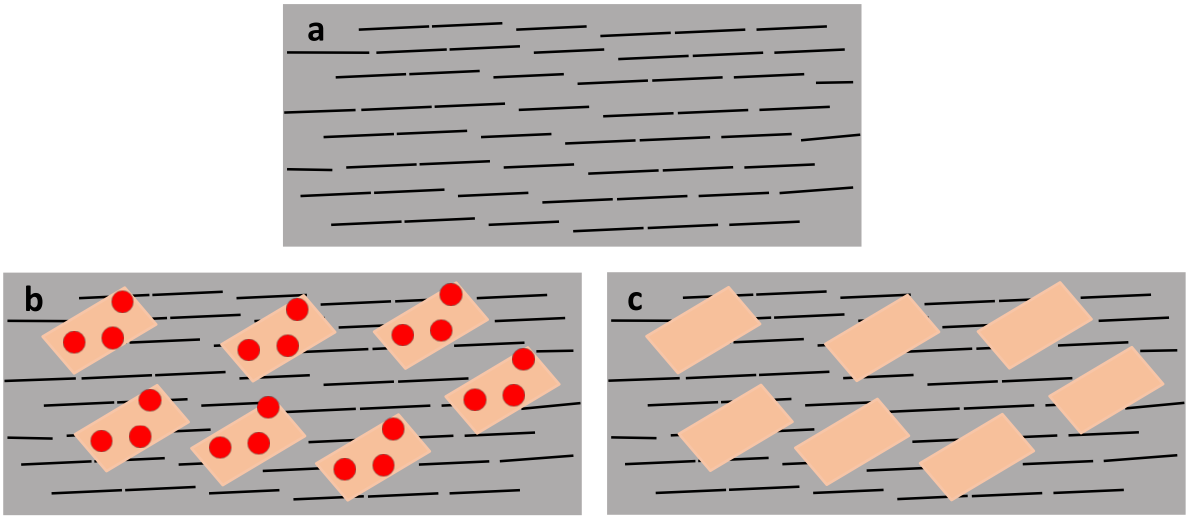

Figure 33. Model for the neat CNT (a), CNT/GO (b), and CNT/rGO (c) fibers.

Figure 33 (b) shows how the GO plates increase the contact between CNT rods far away from each other. The red dots in Figure 33 (b) indicate the presence of oxygen containing functional groups, and helps to explain why the interactions between the CNTs and the GO sheets is not highly favorable. However, for the CNT/rGO combination as shown in Figure 33 (c), the functionality is removed allowing for favorable VDW interactions between the rGO plates and the CNTs. The fiber fracture morphology was also determined via SEM and is shown in Figure 34.

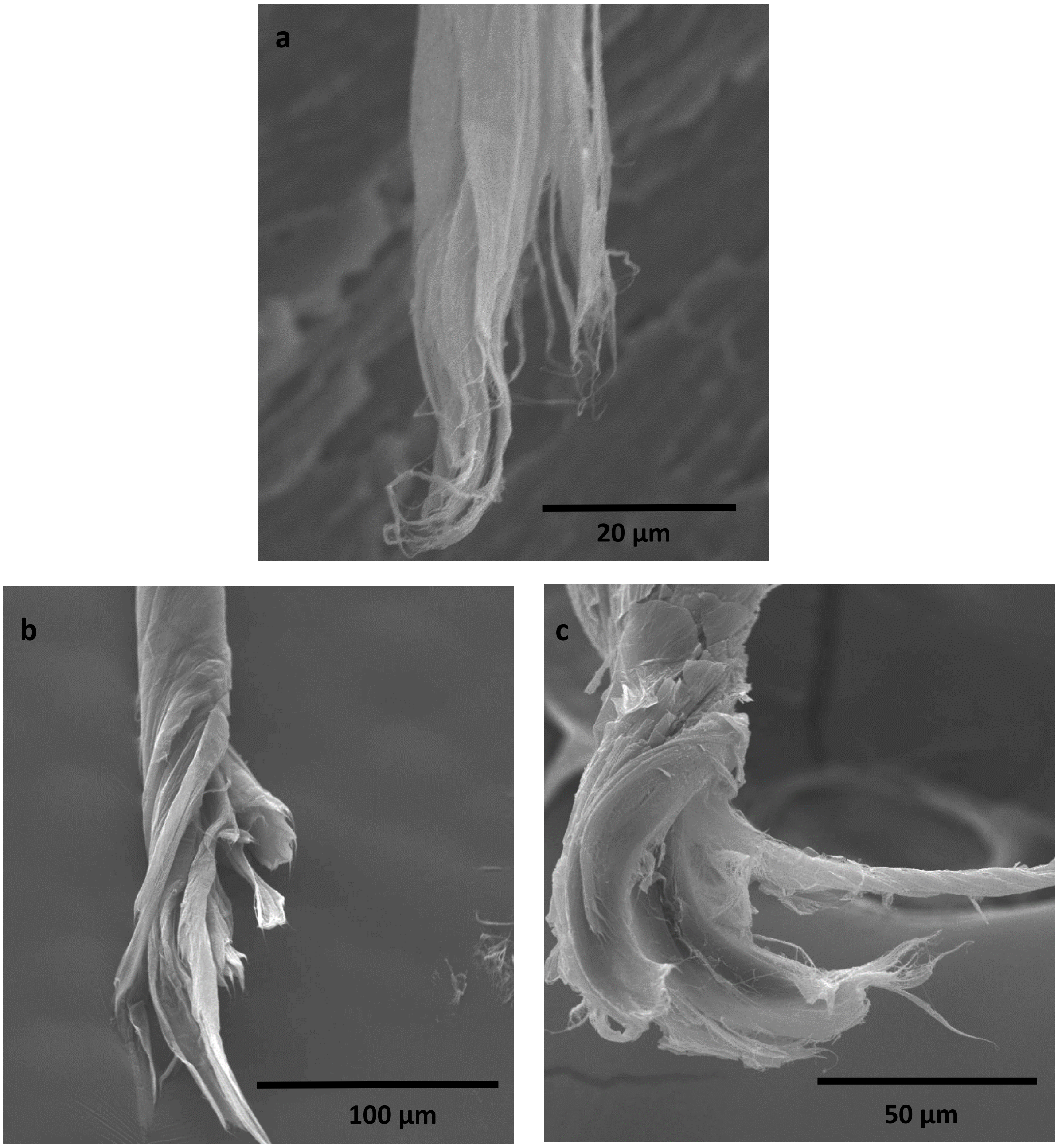

Figure 34. Fiber fracture morphology for the neat CNT (a), CNT/GO (b), and CNT/rGO (c) fibers.

The fiber fracture morphology for neat CNT fibers shown in Figure 34 (a) demonstrates how the neat CNT fibers typically frayed. They typically appeared slightly unraveled with frayed edges along the unraveled strands. Figure 34 (b) shows how the CNT/GO fibers have much more elongated fracture morphologies. In general, the CNT/GO fibers did not unravel and instead display necking. The CNT/rGO fractures generally also displayed necking and more elongated fractures than the neat CNT fibers as shown in Figure 34 (c). These results are consistent with the proposed model and demonstrate how the presence of GO or rGO sheets can alter the way in which the fiber fractures.

3.3 Microfluidic Spun GO LC Fibers

For the wet-spun GO LC fibers, POM was used to characterize the LC phase, SEM was used to determine fiber morphology, and DMA was used to determine the mechanical properties of the prepared fibers. It is worth noting that many of the fibers were so brittle and full of visible defects that they did not produce decent data regarding their mechanical properties. Various ways to improve upon the problems associated with this technique will be discussed in future work. A GO LC phase diagram was constructed for the original 4.5 hour batch of GO as shown in Figure 35.

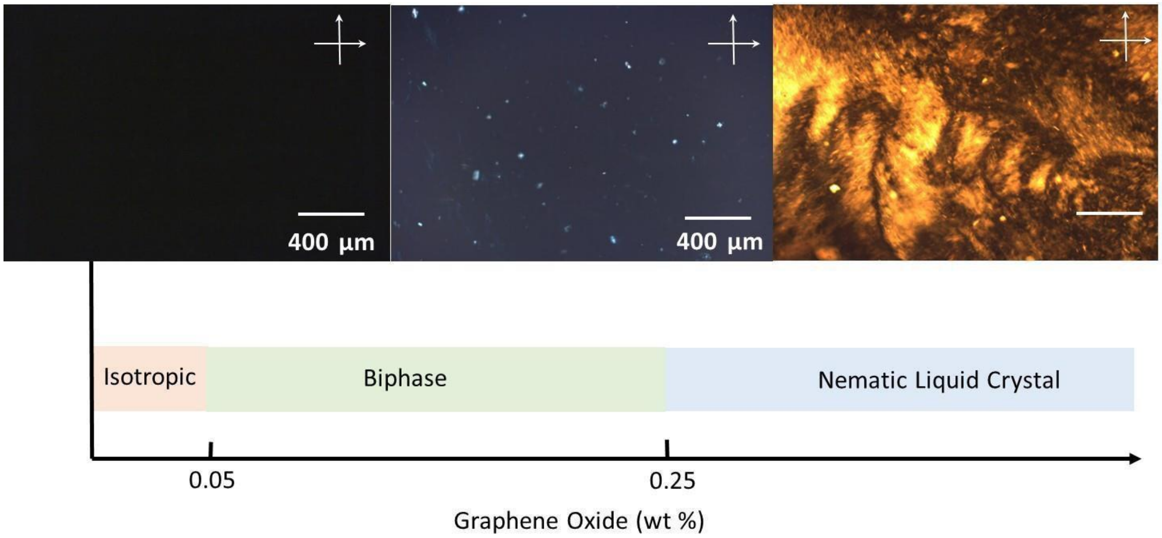

Figure 35. A GO LC phase diagram of the 4,5 hour batch of GO.

First, the GO gel-like product was made into films in triplicate that were dried overnight in a desiccator, and the average concentration was determined to be 1.45% GO (by wt.). Various dispersions were prepared with the 1.45% (by wt.) dispersion, and they were observed via POM to narrow down the I-B and B-N transition. As shown in

Figure 33, the I-B transition occurs at around 0.05% GO (by wt.), and the B-N transition occurs at around 0.25% GO (by wt). These results are fairly consistent with past studies, and phase boundaries are expected to vary depending on size and polydispersity of the sample.[22] Once the LC phase transitions were determined, 1:2 and 1:4 dilutions were prepared in either DI H_2O or EtOH to determine what type of GO LC dope would perform most optimally. Note that the original 1.45% GO (by wt.) dispersion was not used directly. Previous studies suggest higher concentrations of GO LCs lead to more optimal mechanical properties using traditional wet-spinning.[21] However, since a microfluidic channel was used to increase the orientation of the GO sheets, lower concentrations were used so that the dispersions could flow more freely in the channel. The different dopes were used in a 100 µm X 75 µm channel, at a speed of 0.1 mL/hr, using a 5% $Zn(NO_3)_2$ in IPA solution as the coagulation bath. In the first batch, there appeared to be contamination on the fibers from the coagulation bath, so all fibers were rinsed in DI water and dried before being imaged. SEM images for the four different GO LC dopes is shown in Figure 36.

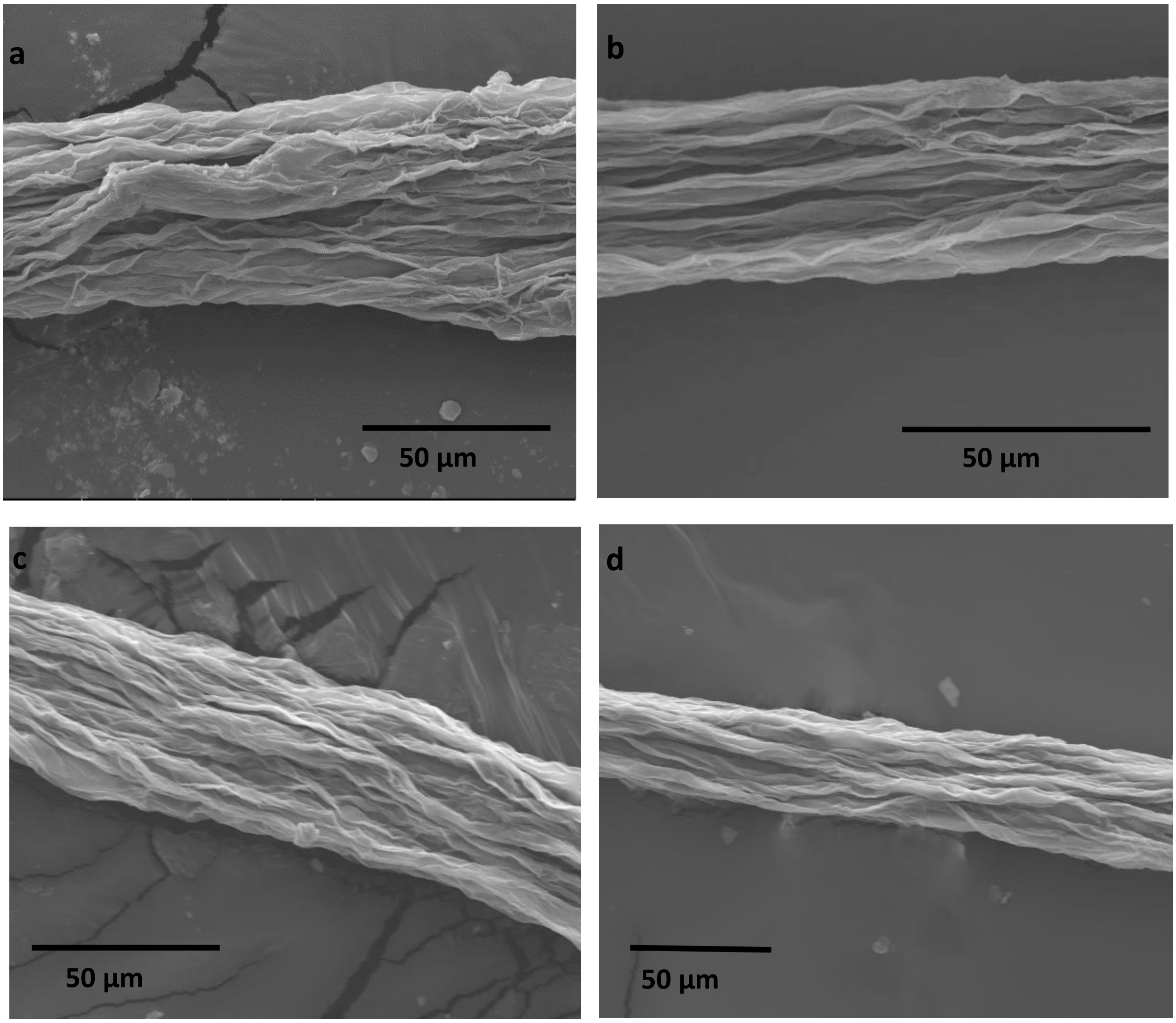

Figure 36. SEM images of fibers using the 0.728 % GO (by wt.) in EtOH (a), the 0.364 % GO (by wt.) in EtOH (b), the 0.728 % GO (by wt.) in DI H_2O (c), the 0.364 % GO (by wt.) in DI H_2O (d).

The average fiber diameters were determined using Image J software. For the EtOH dispersions the diameters were 54.6 and 38.9 µm for the 0.728 % GO (by wt.) and for the 0.364% GO (by wt.) dispersions respectively. The DI H_2O dispersions prepared were shown to have slightly smaller average diameters of 46.7 and 33.8 µm for the 0.728 % GO (by wt.) and for the 0.364 % GO (by wt.) dispersions respectively. The results are summarized in Table 2. The DI H_2O dispersions also appeared to be more consistent in diameter. EtOH is more volatile than H_2O, so the GO sheets in those fibers may buckle more quickly thereby producing less consistent, wider fibers. In general, the alignment observed also appeared to be better in the DI H_2O dispersions.

Table 2. Average diameter for GO LC fibers prepared at 0.1 mL/hr using a 100 X 75 µm channel with a 5% $Zn(NO_3)_2$ in IPA coagulation bath.

	Average Diameter (µm)	
	0.728% GO by wt.	0.364% GO by wt.
EtOH	54.6	38.9
H_2O	46.7	33.8

The next GO LC fiber batch was prepared under the following conditions: a 0.364% GO (by wt) in DI H_2O LC dope was used, in a 100 X 75 µm channel, using a flow rate of either 1 or 10 mL/hr, and using one of three coagulation baths. The purpose was to determine what effect the coagulation bath had on morphology and mechanical properties. Again, a large majority of the fibers were too brittle to obtain decent stress-strain curves, so only the morphology was able to be effectively compared. Figure 37 shows typical SEM images of the prepared fibers, and the diameter results, determined using Image J software, are summarized in Table

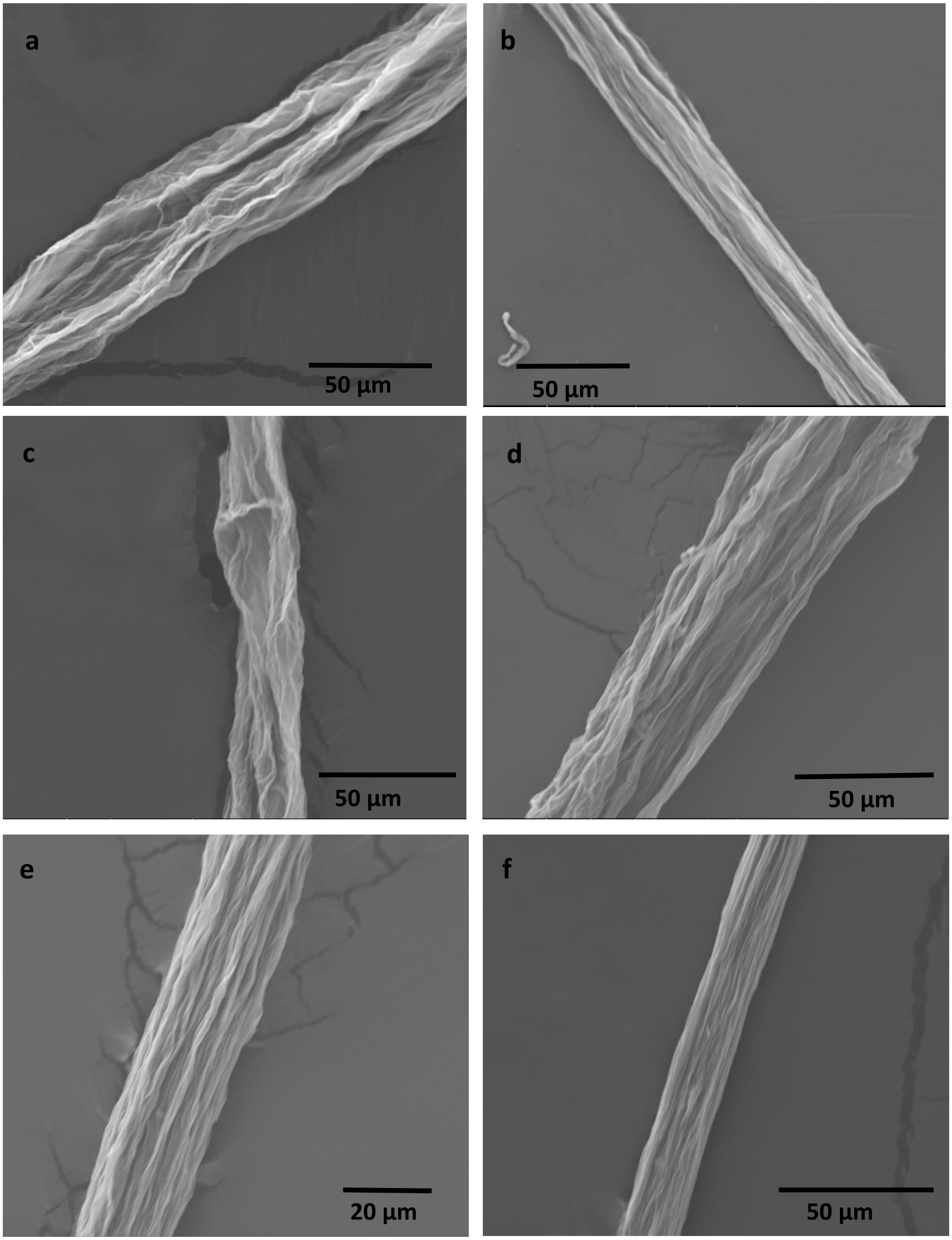

Figure 37. GO LC fibers prepared in a 5 % $Zn(NO_3)_2$ in IPA solution (a) & (b), in a 5 % $CaCl_2$ in EtOH solution (c) & (d) , and in a $CaCl_2$ in IPA solution (e) & (f). Fibers were prepared at either 1 mL/hr (a), (c), & (e), or at 10 mL/hr (b), (d), & (f).

Table 3. Average diameter for GO LC fibers prepared with a 0.364 % GO (by wt.) aqueous dispersion, using a 100 X 75 µm channel at varying flow rates and in varying coagulation baths.

	Average Diameter (µm)	
	1 mL/hr	10 mL/hr
5 % $Zn(NO_3)_2$ in IPA	31.7	27.1
5 % $CaCl_2$ in EtOH	27.2	25.1
5 % $CaCl_2$ in IPA	28.6	22.0

In general, the 5 % $CaCl_2$ in IPA coagulation bath resulted in fibers with relatively smaller diameters that also appeared to have the best alignment, based on the SEM images. Alignment also appeared to increase with flow rate. An Image J plugin was attempted to be used to quantify the alignment of the fibers, but there was a bug in the code, so the relative alignments were only able to be visually observed. Fibers with poor alignment can be characterized by their wavy textured bands, while fibers with better alignment appear to have more linear shaped bands. All of the fibers are wrinkled, but the ones with poorer alignment display much larger wrinkles. The diameter of the fibers was also shown to decrease with increasing speed. From this point forward, the 5% $CaCl_2$ in IPA coagulation bath was used with a 0.364% GO (by wt.) aqueous dispersion, using flow rates near 10 mL/hr. The next batch of prepared fibers investigated the effect of channel size and flow rate. There were not always clear trends, which can be attributed to the fact that these fibers are drawn up by hand, and thereby vary from one another considerably. Again, the mechanical properties were attempted to be determined but the results were very inconsistent and were also difficult to correct due to high variability in cross-sectional area. Another correction method using force divided by linear density was attempted, but it resulted in unreasonably high values. The GO LC fibers are likely not fully densified, meaning there is space between the GO sheets, which may be why this correction method led to an obvious overestimation of mechanical properties. That being said, the morphology was analyzed for cross-sectional shape and alignment, and some representative SEM images are displayed in Figure 36.

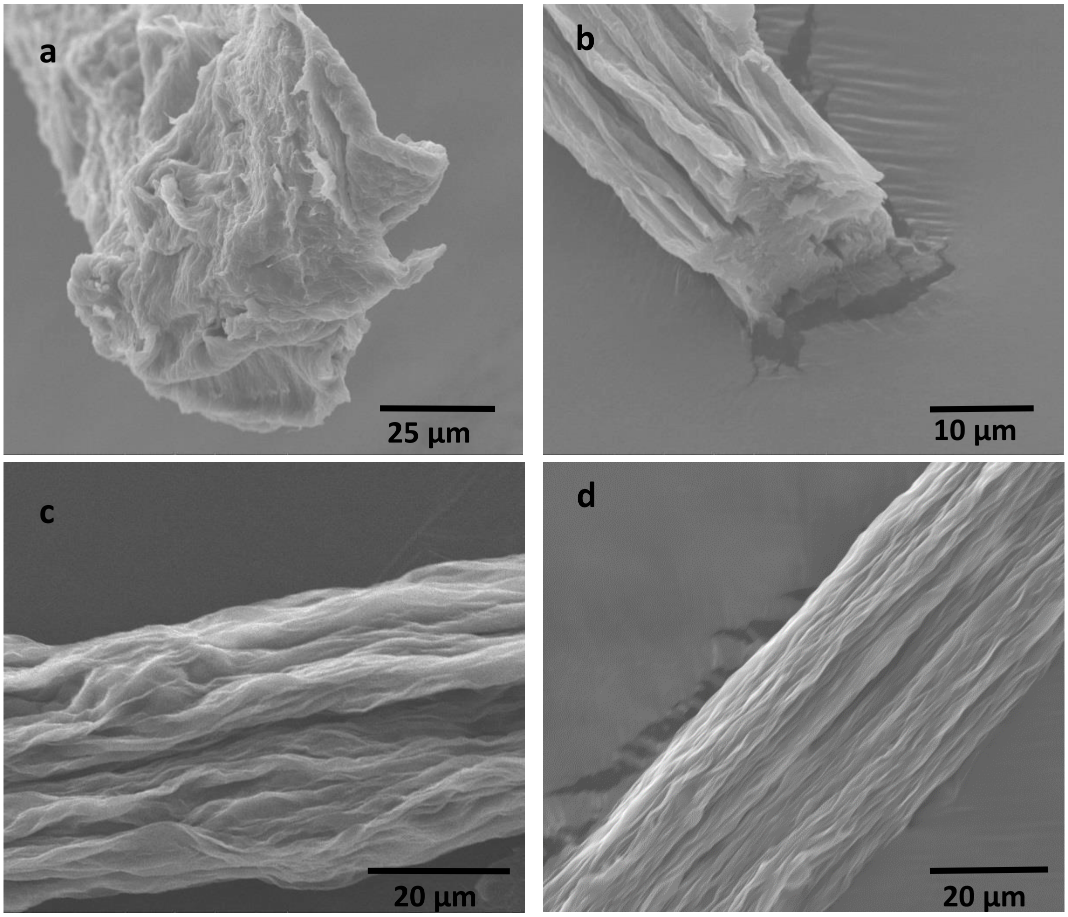

Figure 38. GO LC fibers prepared in a 50 X 100 µm channel at 40 mL/hr (a), in a 75 X 100 µm channel at 2.5 mL/hr (b), in a 200 X 100 µm channel at 5 mL/hr (c), and in a 75 X 100 µm channel at 40 mL/hr.

Figure 38 (a) and (b) show the variation in cross-section depending on the parameters used during preparation. Overall, fibers prepared at higher speeds had more planar cross sections, while fibers prepared at lower speeds had more circular cross sectional areas. Channel width did not appear to have as much of an impact of cross-section morphology for fibers prepared at lower speeds, but for fibers prepared at higher speeds, the cross-section was even more planar for fibers prepared in larger channels. Figure 38 (b) and (d) allows for the examination of how alignment is affected by flow rate and channel size. Fibers prepared using higher flow rates typically appeared to have greater alignment, while fibers prepared using slower flow rates did not appear to be as aligned. Again, channel size did not appear to have as much of an impact, but alignment was generally more optimal in smaller channels. The alignment of the high rate fibers was desirable, but their planar cross sections were not. So, fibers were prepared at high flow rates, and some were twisted in an attempt to before drying under IR light. The twisting was expected to result in a more circular and more consistent structure. It was also expected to result in stronger fibers, because twisting can increase the load bearing ability of the fiber. Variables such as length of fiber, speed of the motor, and time spent spinning were kept constant in order to avoid too much variation between fibers. The length was kept to approximately 10 cm per fiber, and each fiber was spun for 90 seconds. The twisted fibers were expected to enhance the mechanical properties because the twisting should ensure the fiber is more uniform. But, in reality the twisted fibers were generally more difficult to work with and they did not consistently have better mechanical properties. For the most part, none of the fibers displayed optimal properties. The fiber with the best mechanical properties was prepared in a 100 X 100 µm channel using a flow rate of 20 mL/hr, and it was not twisted. The twisted fibers may have actually increased the number of defects resulting in poorer mechanical properties. The corrected stress strain curve obtained using a force ramp of 0.007 N/min is shown in Figure 39, and SEM images showing the fiber cross section and alignment are shown in Figure 40. It is worth mentioning that this curve was corrected by assuming the cross-section was consistent throughout the fiber even though it did not appear to be entirely consistent. Also, while these results were much better than any previously obtained, they were not reproducible.

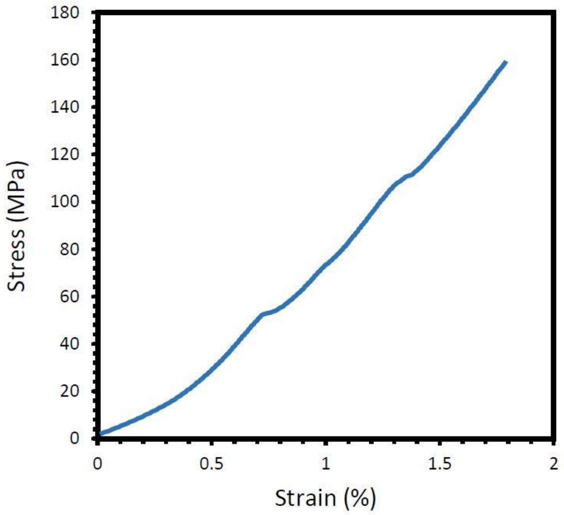

Figure 39. Stress-strain curve for GO LC fiber with the most optimal mechanical properties.

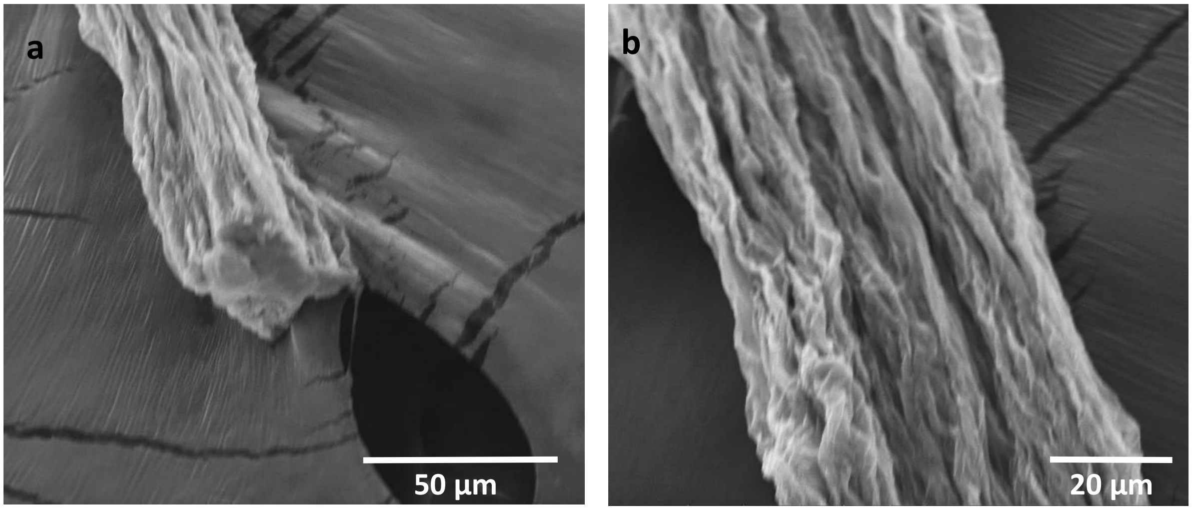

Figure 40. Cross-section (a), and alignment (b) SEM images for the GO LC fiber with the most optimal mechanical properties.

As shown in Figure 40 (a), the fiber appears to have a rectangular cross section. The cross section dimensions were measured using image J software and the cross-sectional area was determined to be $5.98 * 10^{-4}$ mm^2. The static force was divided by this cross-sectional area to obtain the stress-strain curve. The tensile strength was determined to be 160 MPa, with a modulus of 2290 MPa, and an elongation of 1.80%. These results are on par with previous literature reports of wet-spun GO LC fibers.

Interestingly, this fiber did not appear to have the best alignment compared to the other fibers. This suggests that more optimal mechanical properties can be obtained with greater alignment. The existing fibers with high alignment were likely fracturing due to other reasons, such as defects. It was mentioned previously that the GO sheets may pin to the walls of the microfluidic device causing defects. When the fibers were prepared, the microfluidic channels often became clogged indicating the GO sheets did have the tendency to stick to the channel walls. In an attempt to visualize this phenomenon, POM images were taken while the GO LC dispersion was pumped through a channel as shown in Figure 41. The largest channel, a 205 X 100 µm sized channel and a low speed of 1 mL/hr was used, because otherwise the images were difficult to visualize with the available microscope and camera.

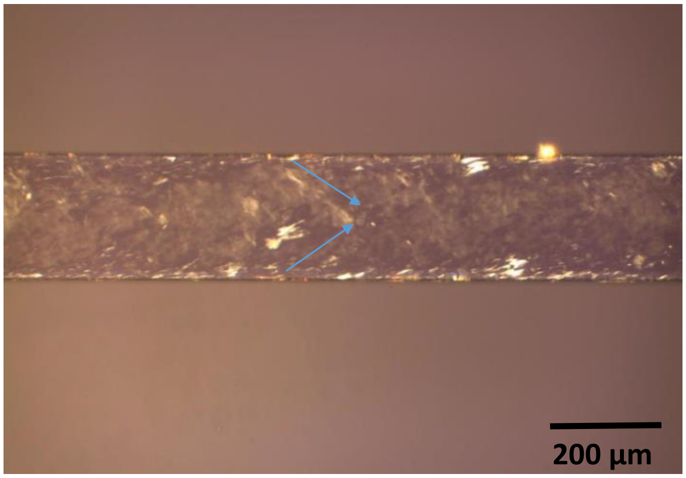

Figure 41. POM image of GO LC dispersion in a microfluidic channel.

Figure 41 clearly shows how the GO sheets homeotropically anchor onto the side walls, thereby producing a defect that has been highlighted with the blue arrows. Also, the original batch of GO was shown to have been over-oxidized resulting in the presence of many disclinations. Overall, the starting material appeared to contain many defects, which the microfluidic channel can add to, resulting in fibers with poor mechanical properties. The disclinatons caused by the channel are unavoidable, but the starting material could possibly be improved to reduce the amount of defects. A few batches of fibers were attempted with the new, 3.5 hour batch, of GO. The new GO batch was determined to have a much higher concentration of 2.34% GO (by wt.). For the new fibers, a 0.585% GO (by wt.) aqueous dispersion was used, and the mechanical properties appeared to be better than fibers prepared with the old batch of GO. The fibers prepared with a 50 X 100 µm channel at 10 mL/hr were compared to fibers prepared without a channel in triplicate and the results are summarized in Table 4, and a representative stress strain curve is shown in Figure 42 along with representative SEM images in Figure 43.

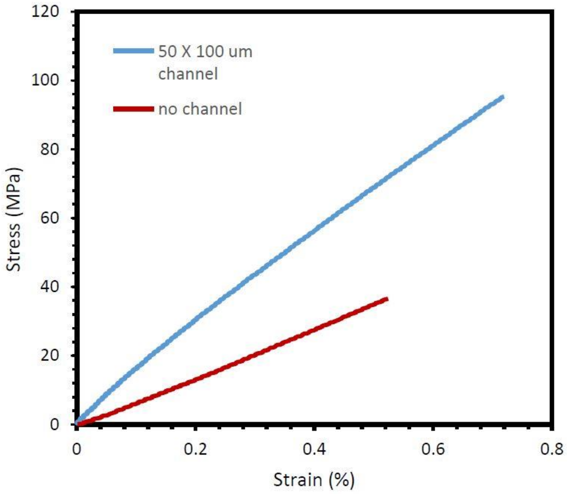

Figure 42. Representative stress-strain curve for GO LC fibers made with a microfluidic channel and without.

Table 4. Summary of average mechanical properties for GO LC fibers prepared with and without a microfluidic channel.

Parameter	Tensile Strength (Mpa)	Modulus (Gpa)	Elongation (%)	Toughness (J/g)
50 X 100 μm Channel	128	2.52	0.914	0.632
No Channel	39.4	0.576	0.737	0.127

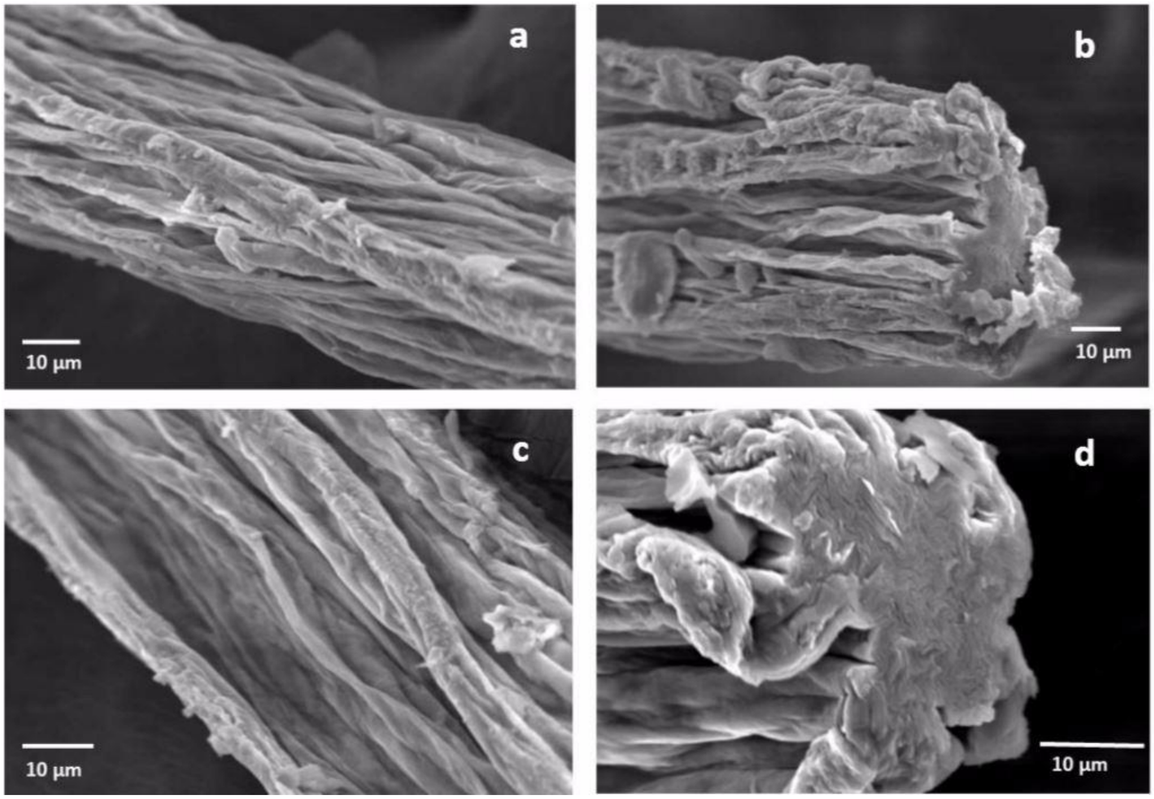

Figure 43. SEM images of a GO LC fiber prepared in a 50 X 100 um channel (a) & (b), and prepared with no channel (c) & (d).

Figure 43 shows how the GO LC fibers have blunt cross-sections implying they are more brittle compared to the CNT aerogel-based fibers. Interestingly, the alignment and cross-section are fairly similar for the fibers made with and without a microfluidic channel. That being said, the fibers prepared in a channel displayed enhanced mechanical properties. They displayed an increased tensile strength, modulus, elongation and toughness when compared to the fiber prepared with no channel. The alignment of the fibers prepared in the channel still does not appear ideal. This means that in the future the fibers prepared in the channel may be further optimized by improving the alignment. Hybrid GO LC/ oCNT fibers were never prepared because there were a lot of difficulties combining the two materials. Figure 44 shows POM images depicting the mix of GO and oCNTs using various techniques to achieve sufficient dispersability.

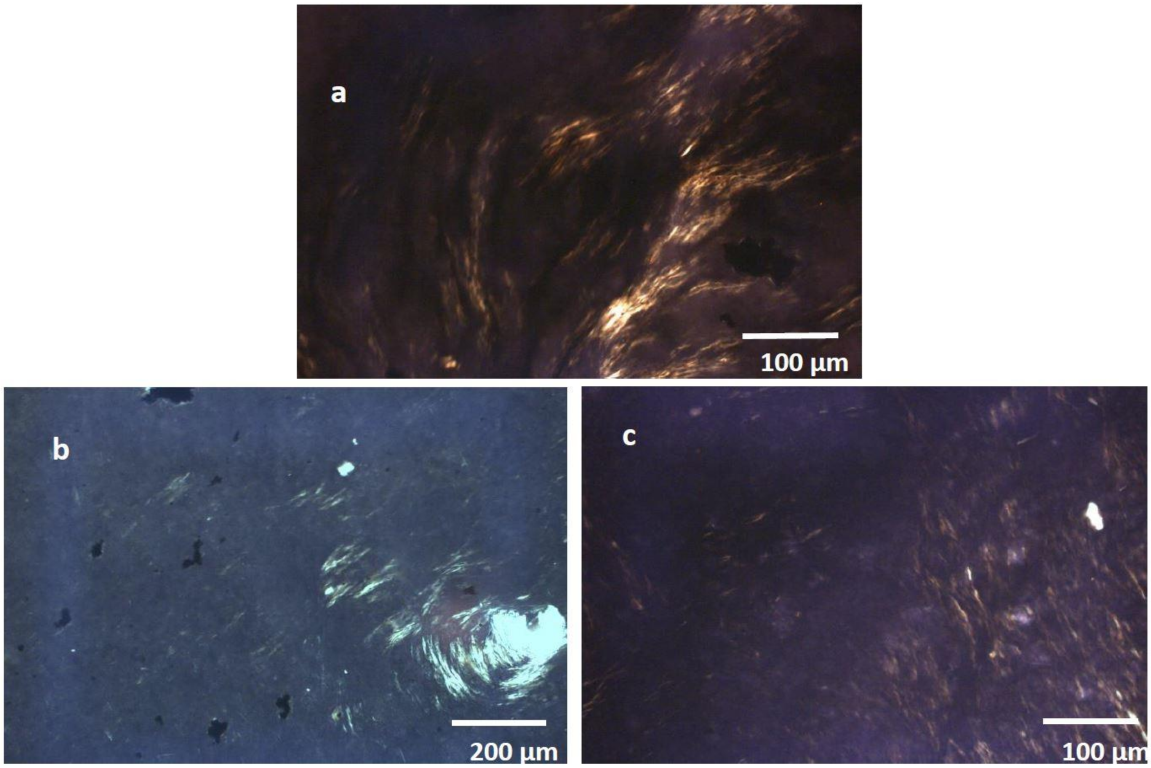

Figure 44. POM images of GO LCs mixed with oCNTs with no treatment (a), with sonication for 1 hour (b), with centrifugation & sonication for 1 hour (c).

Figure 44 (a) shows large CNT aggregates whose size was shown to be reduced in Figure 44 (b) following sonication. Ultimately, the oCNTs were only dispersible after they had been centrifuged at 10,000 RPM for 1 hour and the supernatant was added to a GO LC to achieve close to a 1:4 dilution. The resulting mixture was 0.46% GO (by wt). Then, the mix was sonicated for an hour followed by vortexing. As shown in Figure 44 (c), this method was successful as there are no visible CNT aggregates and the GO LC structure is still visible. The oCNTs were much more difficult to disperse than expected. Even though it is promising that the addition of the oCNT supernatant was achieved without disrupting the GO LC phase, the oCNTs in the supernantant are likely very short and may not optimize mechanical properties because they will not be able to form many entanglements. These mixed dispersions could only be obtained on a scale of about 0.3 mL, which is not enough materials for processing into a fiber.

4. Conclusion

Overall the characterization methods were able to effectively provide information regarding the general structure of the synthesized products. IR data confirmed the presence of oxygen-containing functional groups in oxidized products, and also showed their absence following reduction of GO. Imaging techniques like AFM, SEM, and optical reflectance were used to observe the relative shape of the oCNTs and GO sheets, which showed evidence of defects, but it was not able to be effectively used to determine their exact size. The Raman spectra showed a thermally reduced GO film to display greater disorder than the GO film implying the reduction causes an increase in defects. The GO batch appeared to have defects implying a possible over-oxidation so a new batch was prepared using a 3.5 hour reaction time, and the 3.5 hour GO batch was shown to have a similar D:G ratio as the previous batch indicating a similar degree of functionalization. XRD was used to show the d-spacing of graphite and GO to be 3.4 and 8.2 Å respectively, which is confirmed by literature. But the rGO did not have a very definitive result implying the reduction may cause damage to the crystalline structure. TGA data was used to verify that the GO underwent a mass loss near 200°C, due to the presence of oxygen functionality, while the rGO did not, implying the thermal reduction was successful in reducing all oxygen groups. Lastly, POM analyses of GO LCs showed a large amount of disclinations, or topological defects in the original 4.5 hour GO batch's structure. The LC texture was compared for the two batches, and the Schlierien texture was more well-defined, with smaller disclinations for the 3.5 hour batch.

Hybrid fibers were successfully prepared via soaking CNT aerogel yarn strands in GO. The CNT/GO and CNT/rGO hybrid fibers both displayed more optimal toughness, but via difference mechanisms. The CNT/GO fibers had the greatest elongation due to sliding between the added GO sheets. The CNT/rGO resulted in the greatest modulus, tensile strength, and toughness. These optimal mechanical properties are achieved because the rGO sheets connect non-neighboring CNTs, which allows for increased load-bearing.

GO LC fibers were effectively prepared via microfluidic spinning. The GO LC I-B phase and B-N phase were determined to be 0.05 and 0.25% GO (by wt.) using POM analyses. 1:2 and 1:4 dilutions were prepared with the original 1.45% GO (by wt) dispersion in either EtOH or DI H_2O to be used as the microfluidic spinning dopes, and their fiber morphology was compared using SEM images and Image J software. The 1:4 dilution in DI H_2O, or 0.364% GO (by wt) aqueous dispersion, was shown to produce the thinnest fibers with an average diameter of 33.8 µm. Flow rates of 1 mL/hr and 10 mL/hr were used in three different coagulation baths and size and alignment was observed. The fibers prepared at 10 mL/hr in a 5% $CaCl_2$ in IPA bath were shown to have the smallest diameter of about 22.0 µm with the best alignment. Then, fibers were prepared at five different speeds in four different channels, but no clear trends were observed likely due to variation caused by drawing the fibers by hand. But in general, higher flow rates of up to 40 mL/hr were shown to have increased alignment, but they were also shown to have planar cross sections. Fibers prepared at flow rates as low as 2.5 mL/hr were shown to have poorer alignment, and inconsistent shape, but have circular cross sections. Channel size was not determined to have as great of an effect on the fiber properties but alignment did appear optimized in the smaller channels. The mechanical properties could not be effectively analyzed, because many of the fibers broke due to defects or were so brittle that they could not be tested. None of the results obtained were reproducible, but the most optimal mechanical performance was observed with a fiber prepared in a 100 X 100 µm channel at 20 mL/hr. The fiber was shown to have a rectangular cross-section and moderate alignment resulting in a tensile strength of 160

MPa,a modulus of 2290 MPa, and an elongation of 1.80%, which is on par with GO LC fibers prepared with traditional wet-spinning methods. The GO used likely contains a large number of defects due to over-oxidation, so a new batch of GO was prepared using a lower oxidation time of 3.5 hours. Fibers were prepared with the new GO, and the resulting fibers prepared using a microfluidic channel had enhanced mechanical properties compared to fibers prepared with no channel. The average tensile strength of the microfluidic spun fibers was 128 MPa, with a modulus of 2.52 GPa, an elongation of 0.914%, and a toughness of 0.652 J/g. Based on the previous morphology studies, the alignment can likely be further improved to prepare fibers with even better mechanical properties. But, microfluidic spinning can also result in particles anchoring in the channel as verified by POM, which is one challenge in using the microfluidic spinning technique. Hybrid fibers were not prepared using this method, because the oCNTs were not easily dispersible in the GO LCs as evidenced by the formation of oCNT aggregates. But when the oCNTs were centrifuged, and only the supernatant was added, the oCNTs could be dispersed in the GO LC with the help of sonication without disrupting the GO LC. So, this mixed dispersion can likely be used as a microfluidic spinning dope once larger amounts are prepared.

The overall results of this work showed various techniques for characterizing nanocarbon materials and proposed two simple, cost-effective methods for preparing nanocarbon fibers. The CNT-aerogel based fibers showed how the combination of graphene and CNT materials results in synergistically enhanced mechanical properties. Initially, there were a lot of challenges associated with the microfluidic spinning of GO LC fibers. But, progress was made in determining the parameters that produced the most optimal fibers in terms of thinness and alignment. The results also suggest that the new batch of GO contains less defects, and the fibers prepared with the new batch were shown to result in reproducible data.

5. Future Work

In terms of the synthesized products, the GO batches may be improved by attempting more gentle oxidation methods. This should result in larger, more uniform GO sheets with more optimal properties. If the starting material can be improved, it will be able to more effectively contribute to optimal mechanical properties in the fibers. In terms of the oCNTs, the reaction time may be lowered to just a few hours in order to try and obtain larger oCNTs. But in this case, the reaction times employed may not be the problem. The starting pristine CNTs claim to have a purity >95%, but often times CNT samples are more impure than they claim to be, so a higher quality CNT sample may need to be purchased.

For the CNT aerogel-based hybrid fibers, the amount of GO loading can be altered to determine what effect that has on mechanical properties. The mechanical properties could also be correlated to GO size. The thermal reduction appeared to lead to crack formation, so other reduction methods like chemical techniques could be used instead. One of the major benefits of high performance nanocarbon fibers is that they can be easily multifunctionalized. So, their thermal or electrical properties could also be analyzed. Additionally, when more materials are available, the fibers may be sewn into fabric or used to make a small electrical device similar to that shown in Figure 12.

For the GO LC fibers, the new 3.5 hour batch of GO appears to lead to reproducible stress-strain curves. So, the most promising conditions from the previous work can be used as a starting point to determine the conditions that produce the fibers with the most optimal mechanical properties. Once determined, various reduction techniques may be used to see what effect that has on the mechanical properties. As mentioned, the oCNTs could be prepared with a short oxidation time, to see if there is improvement in their dispersability when mixed with the GO LC. Another option is to try using pristine CNTs because GO has been shown to effectively disperse pristine CNTs in previous literature reports due to its amphiphilic nature. Similar to the CNT aerogel based fibers, the GO LC based fibers can be multifunctional so their thermal and electrical properties can be studied. They may also be used in textiles or in a miniature electrical device.

REFERENCES

1. De Volder, M. F. L., Tawfick, S. H., Baughman, R. H. & Hart, a J. Carbon nanotubes: present and future commercial applications. Science 339, 535–9 (2013).
2. Gao, W. The chemistry of graphene oxide. Graphene Oxide Reduct. Recipes, Spectrosc. Appl. 61–95 (2015). doi:10.1007/978-3-319-15500-5_3
3. Si, Y. & Samulski, E. T. Synthesis of Water Soluble Graphene. 8, 1679–1682 (2008).
4. Shao, Y. et al. Graphene based electrochemical sensors and biosensors: A review. Electroanalysis 22, 1027–1036 (2010).
5. Tian, M. et al. Enhanced mechanical and thermal properties of regenerated cellulose/graphene composite fibers. Carbohydr. Polym. 111, 456–462 (2014).
6. Ni, Z. H. et al. Reflection and Contrast Spectroscopy Graphene Thickness Determination Using Reflection and Contrast Spectroscopy. Nano (2007). doi:10.1021/nl071254m
7. Gómez-Navarro, C. et al. Atomic structure of reduced graphene oxide. Nano Lett. 10, 1144–1148 (2010).
8. William S. Hummers, J. & Offeman, R. E. Preparation of Graphitic Oxide. J. Am. Chem. Soc 80, 1339 (1958).
9. Lerf, A., He, H., Forster, M. & Klinowski, J. Structure of Graphite Oxide Revisited. J. Phys. Chem. B 102, 4477–4482 (1998).
10. Lee, D. W. et al. 氧化石墨结构表征The Structure of Graphite Oxide Investigation of Its Surface Chemical Groups.pdf. 5723–5728 (2010).

11. Kim, D. H., Yun, Y. S. & Jin, H. J. Difference of dispersion behavior between graphene oxide and oxidized carbon nanotubes in polar organic solvents. Curr. Appl. Phys. 12, 637–642 (2012).

12. Kim, J. et al. Graphene oxide sheets at interfaces. J. Am. Chem. Soc. 132, 8180–8186 (2010).

13. Expandable Flake Graphite | Asbury Carbons. Available at: https://asbury.com/technical-presentations-papers/materials-in-depth/expandable-flake-graphite/. (Accessed: 19th February 2016)

14. Dubin, S. et al. A one-step, solvothermal reduction method for producing reduced graphene oxide dispersions in organic solvents. ACS Nano 4, 3845–3852 (2010).

15. Park, S. et al. Colloidal suspensions of highly reduced graphene oxide in a wide variety of organic solvents. Nano Lett. 9, 1593–1597 (2009).

16. Saifuddin, N., Raziah, A. Z. & Junizah, A. R. Carbon nanotubes: A review on structure and their interaction with proteins. J. Chem. 2013, (2013).

17. Ali-Boucetta, H. et al. Asbestos-like pathogenicity of long carbon nanotubes alleviated by chemical functionalization. Angew. Chemie - Int. Ed. 52, 2274–2278 (2013).

18. Zhang, S. & Kumar, S. Carbon nanotubes as liquid crystals. Small 4, 1270–1283 (2008).

19. Zhang, J. et al. Effect of Chemical Oxidation on the Structure of Single-Walled Carbon Nanotubes. J. Phys. Chem. B 107, 3712–3718 (2003).

20. Wepasnick, K. A. et al. Surface and structural characterization of multi-walled carbon nanotubes following different oxidative treatments. Carbon N. Y. 49, 24–36 (2011).

21. Xu, Z. & Gao, C. Graphene chiral liquid crystals and macroscopic assembled fibres. Nat. Commun. 2, 571 (2011).

22. Luo, Y. et al. Nematic order drives macroscopic patterns of graphene oxide in drying drops. Langmuir 30, 14631–14637 (2014).

23. Zhang, S., Kinloch, I. A. & Windle, A. H. Mesogenicity drives fractionation in lyotropic aqueous suspensions of multiwall carbon nanotubes. Nano Lett. 6, 568– 572 (2006).

24. Xu, Z. & Gao, C. Aqueous Liquid Crystals of Graphene Oxide SI. ACS Nano 5, 1– 8 (2011).

25. Zhang, S., Terentjev, E. M. & Donald, A. M. Disclinations and their interactions in thin films of side-chain liquid crystalline polymers. Macromolecules 37, 390–396 (2004).

26. Håkansson, K. M. O. et al. Hydrodynamic alignment and assembly of nanofibrils resulting in strong cellulose filaments. Nat. Commun. 5, 4018 (2014).

27. Chae, S. K., Kang, E., Khademhosseini, A. & Lee, S. H. Micro/nanometer-scale fiber with highly ordered structures by mimicking the spinning process of silkworm. Adv. Mater. 25, 3071–3078 (2013).

28. Sengupta, A., Tkalec, U. & Bahr, C. Nematic textures in microfluidic environment. Soft Matter 7, 6542 (2011).

29. Guo, F. et al. Hydration-responsive folding and unfolding in graphene oxide liquid crystal phases. ACS Nano 5, 8019–8025 (2011).

30. Vanakaras, a. G. & Photinos, D. J. Theory of Biaxial Nematic Ordering in Rod- Disc Mixtures Revisited. Mol. Cryst. Liq. Cryst. Sci. Technol. Sect. A. Mol. Cryst. Liq. Cryst. 299, 65–71 (1997).

31. Puech, N. et al. Highly Ordered Carbon Nanotube Nematic Liquid Crystals. J. Phys. Chem. C 115, 3272–3278 (2011).

32. High Performance Carbon Fibers - National Historic Chemical Landmark - American Chemical Society. Available at: http://www.acs.org/content/acs/en/education/whatischemistry/landmarks/carbonfibers.html. (Accessed: 19th February 2016)

33. Xu, Z. & Gao, C. Graphene fiber: A new trend in carbon fibers. Mater. Today 18, 480–492 (2015).

34. Xu, Z. & Gao, C. Graphene in macroscopic order: Liquid crystals and wet-spun fibers. Acc. Chem. Res. 47, 1267–1276 (2014).

35. Dong, Z. et al. Facile fabrication of light, flexible and multifunctional graphene fibers. Adv. Mater. 24, 1856–1861 (2012).

36. Cheng, H. et al. Moisture-activated torsional graphene-fiber motor. Adv. Mater. 26, 2909–2913 (2014).

37. Behabtu, N. et al. Strong, light, multifunctional fibers of carbon nanotubes with ultrahigh conductivity. Science (80-.). 339, 182–6 (2013).

38. Jiang, C. et al. Macroscopic Nanotube Fibers Spun from Single-Walled Carbon Nanotube Polyelectrolytes. ACS Nano 8, 9107–9112 (2014).

39. Zhang, X. et al. Ultrastrong, stiff, and lightweight carbon-nanotube fibers. Adv. Mater. 19, 4198–4201 (2007).

40. Li, Q. et al. Sustained growth of ultralong carbon nanotube arrays for fiber spinning. Adv. Mater. 18, 3160–3163 (2006).

41. Koziol, K. et al. High-performance carbon nanotube fiber. Science (80-.). 318, 1892–5 (2007).

42. Alemán, B., Reguero, V., Mas, B. & Vilatela, J. J. Strong Carbon Nanotube Fibers by Drawing Inspiration from Polymer Fiber Spinning. ACS Nano 9, 7392–7398 (2015).

43. Motta, M., Li, Y. L., Kinloch, I. a. & Windle, a. H. Spun fibers of carbon nanotubes. Nano Lett. 5, 1529–1533 (2005).

44. Zhang, S. et al. Solid-state spun fibers and yarns from 1-mm long carbon nanotube forests synthesized by water-assisted chemical vapor deposition. J. Mater. Sci. 43, 4356–4362 (2008).

45. Shin, M. K. et al. Synergistic toughening of composite fibres by self-alignment of reduced graphene oxide and carbon nanotubes. Nat. Commun. 3, 650 (2012).

46. Meng, F. et al. Multifunctionalization of carbon nanotube fibers with the aid of graphene wrapping. J. Mater. Chem. 22, 16277 (2012).

47. Sun, H. et al. Novel graphene/carbon nanotube composite fibers for efficient wire-shaped miniature energy devices. Adv. Mater. 26, 2868–2873 (2014).

48. Ma, Y. et al. Conductive graphene fibers for wire-shaped supercapacitors strengthened by unfunctionalized few-walled carbon nanotubes. ACS Nano 9, 1352-1359 (2015).

49. Paredes, J. I., Marti, a, Tasco, J. M. D. & Martı, a. Graphene Oxide Dispersions in Organic Solvents Graphene Oxide Dispersions in Organic Solvents. 24, 10560–10564 (2008).

50. Gaskell, P. E., Skulason, H. S., Rodenchuk, C. & Szkopek, T. Counting graphene layers on glass via optical reflection microscopy. Appl. Phys. Lett. 94, 14–17 (2009).

51. Microanalysis, X., Goldstein, J. I., Newbury, D. E., Lyman, C. E. & Joy, D. C. Microscopy and Scanning Electron Microscopy and A Text for Biologists. (1992).

52. Kudin, K. N. et al. Raman spectra of graphite oxide and functionalized graphene sheets. Nano Lett. 8, 36–41 (2008).